

Journal of Geophysical Research: Solid Earth

RESEARCH ARTICLE

10.1002/2017JB014080

Key Points:

- Northward younging trend in cooling ages of Xigaze fore-arc basin
- Exhumation history linked to changes in India-Asia convergence rates
- Sedimentation in Xigaze basin probably continued until latest Eocene

Supporting Information:

- Supporting Information S1

Correspondence to:

G. Li,
guangwei.li@unimelb.edu.au

Citation:

Li, G., B. Kohn, M. Sandiford, and Z. Xu (2017), India-Asia convergence: Insights from burial and exhumation of the Xigaze fore-arc basin, south Tibet, *J. Geophys. Res. Solid Earth*, 122, 3430–3449, doi:10.1002/2017JB014080.

Received 7 FEB 2017

Accepted 6 APR 2017

Accepted article online 20 APR 2017

Published online 11 MAY 2017

India-Asia convergence: Insights from burial and exhumation of the Xigaze fore-arc basin, south Tibet

Guangwei Li¹ , Barry Kohn¹ , Mike Sandiford¹, and Zhiqin Xu²

¹The School of Earth Sciences, University of Melbourne, Parkville, Victoria, Australia, ²The Department of Earth Sciences, Nanjing University, Nanjing, China

Abstract The composite fore-arc/syncollisional Xigaze basin in south Tibet preserves a key record of India-Asia collision. New apatite fission track and zircon (U-Th)/He data from an N-S transect across the preserved fore-arc basin sequence near Xigaze show a consistent northward Late Cretaceous to middle Miocene younging trend, while coexisting apatite (U-Th-Sm)/He ages are all Miocene. Corresponding detrital zircon U-Pb data are also reported for constraining the Cretaceous depositional ages of the Xigaze basin sequence in the region. Thermal history modeling indicates that the basin experienced northward propagating episodic exhumation, along with a northward migration of the depocenter and a pre-existing Cenozoic syncollisional basin sequence which had been removed. In the southern part, fore-arc exhumation commenced in the Late Cretaceous ($\sim 89 \pm 2$ Ma). Following transition to a syncollisional basin in the Paleocene, sedimentation in the central and northern Xigaze basin continued until the latest Eocene ($\sim 34 \pm 4$ Ma). Ongoing folding and thrusting (e.g., Great Counter Thrusts) caused by progressive plate convergence during late Oligocene-early Miocene time resulted in regional uplift and considerable basin denudation, which fed two fluvial basins along its northern and southern flanks and exposed the basement ophiolite. Subsequent incision of the Yarlung River resulted in Miocene cooling in the region. Different episodes in the exhumation history of the Xigaze basin, caused by thrusting of an accretionary wedge and ophiolitic basement, can be linked to changes in India-Asia convergence rates and the changing subduction pattern of the Indian and Neo-Tethyan slabs.

1. Introduction

Subduction-related fore-arc and collision-related syncollisional basins located on the continental margin preserve significant information regarding the erosional and magmatic records of continental margins and the pre/syn/postcollisional history between continents and therefore form important archives of continental dynamics [DeCelles *et al.*, 2011; Noda, 2016]. Along the southern margin of the Asian plate, the Xigaze basin includes a fore-arc basin that transitioned into a syncollisional basin following collision [e.g., DeCelles *et al.*, 2014]. While much of the younger syncollisional basin component was denuded during subsequent regional uplift, the thermal imprint revealed by the thermochronological history of preserved basin sediments potentially provides a unique record of India-Asia convergence.

The Xigaze fore-arc basin, also known as the Gangdese fore-arc basin, preserves a >4 km thick sedimentary section and was formed along the Indus-Yarlung Suture Zone in the Himalayan orogenic belt. It extends laterally for ~ 600 km across southern Tibet, linking up with a coeval fore-arc basin in Ladakh further west [Hu *et al.*, 2016b; Garzanti and van Haver, 1988] (Figure 1). The younger basin sequence is only partly preserved in SW Tibet near Zhongba (Figure 1). Previous work has included studies of paleontology, sedimentology, petrography, and provenance analysis and mainly focused on depositional processes [e.g., Einsele *et al.*, 1994; Dürr, 1996; An *et al.*, 2014; Orme *et al.*, 2014]. The postdepositional uplift and exhumation history of the basin during the course of India-Asia collision, however, has received very little attention. Further, the timing of structural emplacement of the suprasubduction zone (SSZ) Xigaze ophiolite, which is considered as basement to the basin [Wang *et al.*, 2012; Huang *et al.*, 2015; Maffione *et al.*, 2015], is not well constrained.

Low-temperature (low-T) thermochronology methods, including zircon/apatite U-Th/He (ZHe and AHe, respectively) and apatite fission track (AFT), have been widely used to reconstruct burial histories and exhumation processes of sedimentary basins [e.g., Garver *et al.*, 1999; Armstrong, 2005]. Here we present a suite of low-T thermochronology data for locations covering an N-S sampling transect across the Xigaze fore-arc

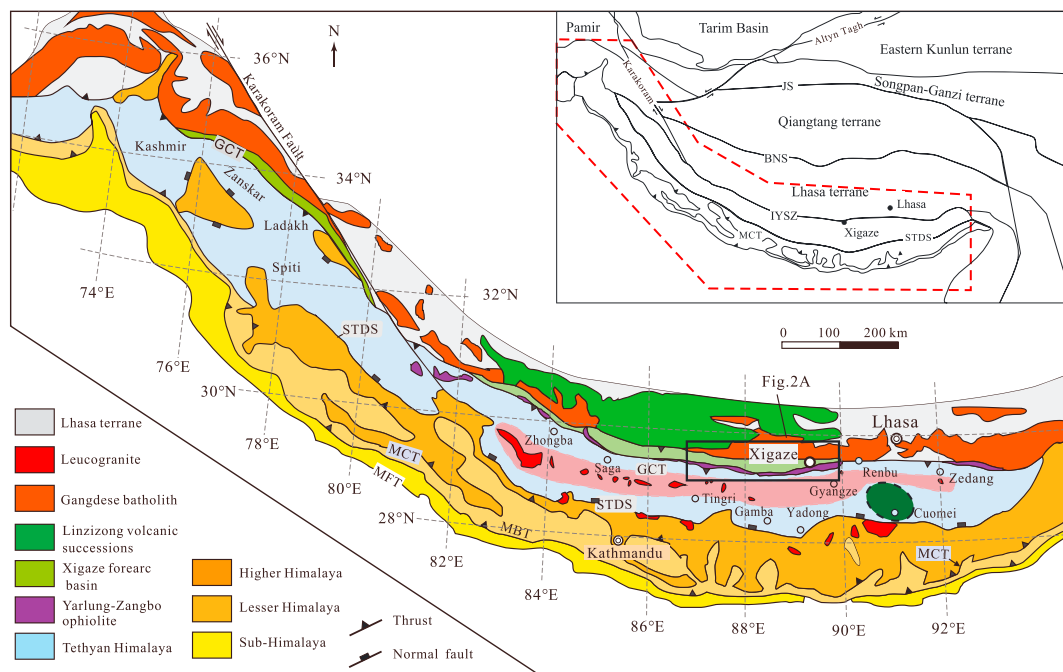


Figure 1. Simplified geological map of the Himalaya orogeny (modified after Yin [2006]). The dark green dashed circle represents the location of the Cuomei LIP [Zhu et al., 2013]; the leucogranites in Tethyan Himalaya (marked as a pink belt) formed the Northern Himalaya gneiss domes (NHGD) [Zeng et al., 2011].

basin near Xigaze (Figures 1 and 2), which is a the widest and most continuous exposed record of the well-studied lower basin Cretaceous sequence [e.g., Einsele et al., 1994; Wan et al., 1998; Wang et al., 2012; An et al., 2014] and is likely to provide a more complete thermal history record. These data are used to constrain the burial and exhumation history of the basin from Cretaceous time, particularly following the initial India-Asia collision at about $\sim 59 \pm 1$ Ma (according to studies on the middle Paleogene Sangdanlin Formation sequence in the Tethyan Himalaya) [e.g., DeCelles et al., 2014; Wu et al., 2014; Hu et al., 2015, 2016a, 2016b], and the process of exhumation of the Xigaze ophiolite. Furthermore, corresponding detrital zircon U-Pb data were

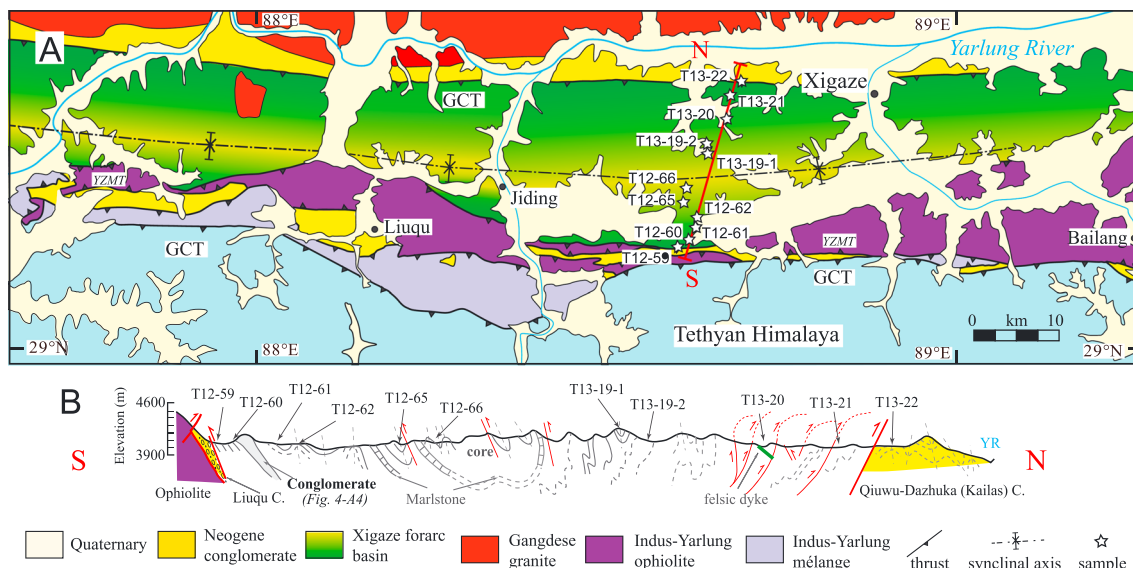


Figure 2. (a) Geologic map of the Xigaze area with sample locations. (b) Structural cross section and sample locations along (N-S) (modified after Einsele et al. [1994] and Wang et al. [2012]), in light of our field observations.

analyzed to determine depositional ages of these Xigaze basin sequences. Together these data shed further light on understanding how continental margins may respond to continental collision through time, in this case relevant to India-Asia collision.

2. Regional Geological Setting

The main India-Asian collision zone in south Tibet separates the Mesozoic-early Cenozoic Asian plate (e.g., Lhasa and Qiangtang terranes) to the north from the Indian plate to the south. From north to south, the zone in the south Tibet mainly comprises the Gangdese arc, Xigaze basin, Indus-Yarlung Suture Zone, and Tethyan, Greater, and Lesser Himalaya (Figure 1). (1) The Gangdese magmatic arc (Trans-Himalaya), extending ~2500 km along the south Asia margin (locally Lhasa terrane), mainly includes plutons and intermediate upper Triassic to upper Miocene volcanic rocks (e.g., Sangri Group, Yeba Formation, and Linzizong Group), which was linked to the Neo-Tethyan oceanic northward subduction [e.g., Schärer *et al.*, 1984; Ji *et al.*, 2009; Zhu *et al.*, 2013]. However, the Triassic-Jurassic magmatism has also been considered as a result of southward subduction of the Bangong-Nujiang Ocean during that time [Zhu *et al.*, 2013]. The latest Oligocene-early Miocene Great Counter Thrust (GCT) or late Oligocene Gangdese Thrust (GC) borders the Gangdese belt to the south [Yin *et al.*, 1999; Murphy and Yin, 2003]. The north-dipping Gangdese Thrust has been proposed as a continuous structure along the entire Gangdese batholith margin [Yin *et al.*, 1999]. However, Aitchison *et al.* [2003] argued for the existence of this thrust along the entire suture zone. (2) The Xigaze basin is composed of deep-marine turbidite-dominated Cretaceous fore-arc Xigaze Group (Chongdui and Ngamring formations) and the shallow marine to nonmarine Paleocene-lower Eocene fore-arc/syncollisional Tso-jiangding Group [Dürr, 1996; An *et al.*, 2014; DeCelles *et al.*, 2014; Orme *et al.*, 2014], which lies on ophiolitic basement [Hébert *et al.*, 2012; Wang *et al.*, 2012; Huang *et al.*, 2015]. (3) The Indus-Yarlung Suture Zone (IYSZ) representing remnants of the Neo-Tethyan oceanic basin consists of ophiolites and associated mélanges [An *et al.*, 2017], which is considered to have formed in a mid-ocean ridge basalt setting during the Jurassic and a supra-subduction setting during the Cretaceous [Malpas *et al.*, 2003; Hébert *et al.*, 2012; Maffione *et al.*, 2015]. Maffione *et al.* [2015] also proposed that the Early Cretaceous suprasubduction ophiolites were formed within the fore-arc hyperextension processes, probably representing melting of subcontinental mantle of the Lhasa terrane. The IYSZ juxtaposes the Xigaze basin and Gangdese arc to the north and the Tethyan Himalayan to the south, marking the boundary between Asian and Indian plates prior to collision (Figure 1). The Yarlung Zangbo Mantle thrust (YZMT), which yields ^{40}Ar - ^{39}Ar cooling age of ~62–63 Ma, represents southward obduction of ophiolitic mélange during early Paleocene [Ding *et al.*, 2005]. The thrust was located on the southern margin of ophiolitic assemblage and was later partially buried by the latest Oligocene to early Miocene thrusting along the Great Counter Thrust (GCT) (Figure 2). (4) The Tethyan Himalaya mainly comprises Cambrian-Eocene low-grade metasedimentary and sedimentary rocks which were deposited along the passive margin of northern India [e.g., Liu and Einsele, 1994; Jadoul *et al.*, 1998; Wan *et al.*, 1998; Garzanti, 1999; Ding *et al.*, 2005], as well as an east-west zone of the Cenozoic Northern Himalayan gneiss domes (NHGD) [e.g., Lee *et al.*, 2004; Lee and Whitehouse, 2007; Zeng *et al.*, 2011; Pullen *et al.*, 2011]. (5) The Greater Himalaya mainly consists of Proterozoic and Paleozoic high-grade metamorphosed metasedimentary rocks locally intruded by Early Paleozoic and Cenozoic granitoids [Parrish and Hodges, 1996; Yin and Harrison, 2000; McQuarrie *et al.*, 2013]. (6) The Lesser Himalaya mainly comprises Proterozoic-Paleozoic metasedimentary rocks, meta-volcanic, and gneiss, overlain by Permian to Cretaceous strata which are similar to the Tethyan Himalayan sequence [e.g., Yin, 2006; DeCelles *et al.*, 2014, and references therein].

Recently, it has been demonstrated that the foreland basin system developed along the entire Himalaya orogeny from the IYSZ to present Gangetic foreland basin. Based on studies from the Sangdanlin section in Saga (Figure 1) combined with previously published data from the IYSZ [Li *et al.*, 2015b], northern Tethyan Himalaya [Ding *et al.*, 2005; Hu *et al.*, 2016b], and frontal Nepalese Lesser Himalaya and Sub-Himalaya [DeCelles *et al.*, 2014], from Paleocene to the present this basin system experienced a flexural wave southward migrating ~1400 km across the Himalayan thrust belt.

3. Sedimentology and Structure in the Xigaze Basin

This work concentrates on the Xigaze fore-arc basin near Xigaze (Figure 2), which mainly preserves the Aptian-Coniacian (~125–80 Ma) Chongdui and Ngamring Formations [Wang *et al.*, 2012; Orme *et al.*, 2014;

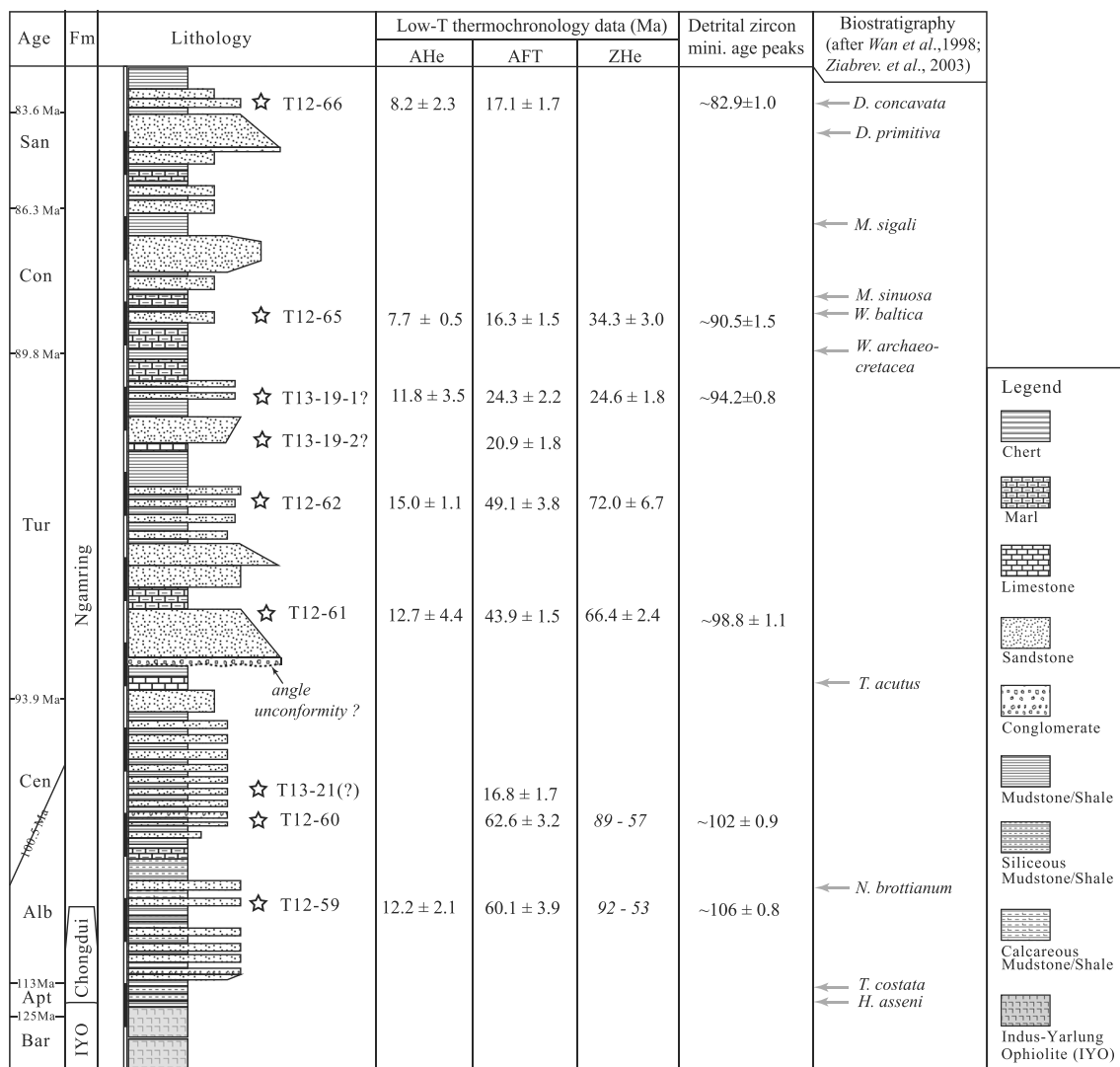


Figure 3. Stratigraphy of the Xigaze fore-arc basin near Xigaze modified after An et al. [2014], showing sample positions, low-T thermochronology data, and minimum detrital zircon U-Pb age peaks (Ma) reported in this study. Alb = Albian, Apt = Aptian, Bar = Barremian, Con = Coniacian, Cen = Cenomanian, San = Santonian, Tur = Turonian.

[Orme and Laskowski, 2016; Figure 3], as well as a small suit of upper Aptian to lower Albian carbonate, Sangzugang Formation, discontinuously exposing in the northern part of the fore-arc basin [Liu et al., 1988; An et al., 2014]. The Chongdui Formation was originally named by Cao [1991] and comprises greenish-purplish upper Barremian and upper Aptian radiolarian chert [Ziabrev et al., 2003], interbedded with tuffaceous layers dated at ~119–114 Ma [Huang et al., 2015; Wang et al., 2017], overlain by grey thin-bedded sandstone, mudstone, and limestone (youngest age of ~116 Ma for detrital zircon U-Pb analyses reported by Wu et al. [2010]; interbedded tuffs with ages of ~113–110 Ma [Wang et al., 2017]). Later, this formation was redefined [An et al., 2014], as only including the lower part: greenish-purplish radiolarian chert intercalated with greenish shale and calcilutite, which is considered to have been deposited over oceanic crust at abyssal depths (Figure 4). The Ngamring Formation overlying conformably the Chongdui Formation (Figure 4) comprises several upward-fining turbidite interlayered with conglomerates [Wang et al., 2012; Orme and Laskowski, 2016]. The depositional age of this formation is still under debate, but biostratigraphic studies [Wan et al., 1998; Li et al., 2010] and detrital zircon U-Pb analyzed constraints [e.g., Wu et al., 2010; An et al., 2014; Orme et al., 2014; Orme and Laskowski, 2016] indicate its depositional age ranges from ~107 to 83 Ma during the Aptian-Turonian. Provenance analysis indicates that the major sediments of the basin were derived from the Gangdese arc [e.g., Dürr, 1996; Wu et al., 2010; Orme et al.,

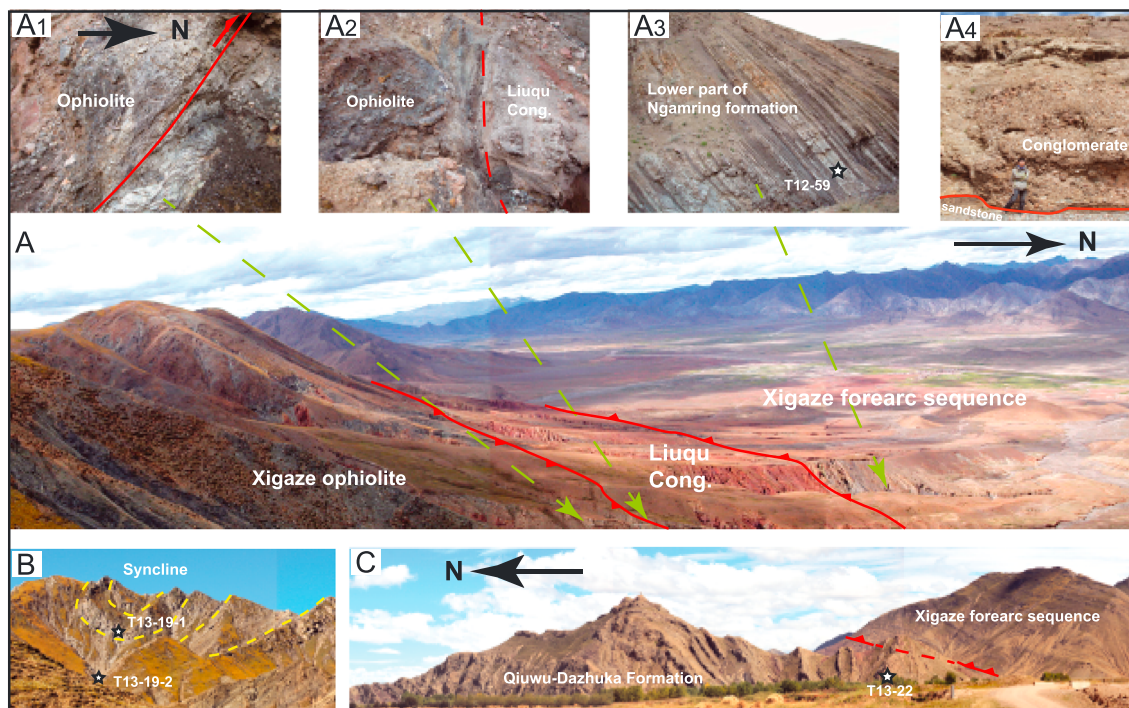


Figure 4. Field features and lithologies of the Xigaze fore-arc basin and adjacent units. (a) Southern Xigaze basin. View toward the west, showing contacts between the Xigaze ophiolite, Liuqu Conglomerate, and Xigaze fore-arc sequence. (a1) Northward thrust in ophiolite body; (a2) contact between ophiolite and Liuqu Conglomerate; (a3) Chongdui Formation, showing location of sample T12-59; (a4) “Channel Conglomerate” in the middle part of the Ngamring Formation (southern basin) shown in Figure 2b. (b) Location of samples (T13-19-1 and T13-19-2) in a syncline in central Xigaze fore-arc basin. (c) Northern Xigaze basin, thrust over latest Oligocene-early Miocene Qiuwu-Dazhuka Formation, showing the location of sample T13-22.

2014]. A >5 m thick conglomerate (Figures 2b, 3, and 4a4) within the middle part of the Ngamring Formation located in the southernmost basin has been interpreted to be deposited in a deepwater channel [Wang et al., 2012; Orme et al., 2014].

Further, those upper Xigaze basin sequences, exposed in the Zhongba-Saga area (Figure 1), named the Tso-jiangding Group, include Jialazi, Quxia, Qubeiya, and Padana formations, range in age from ~83 to 50 Ma [e.g., Wang et al., 2012; An et al., 2014; Orme et al., 2014; Hu et al., 2016b]. This group mainly comprises limestone, interbedded marine sandstone, shale, and conglomerate, indicating a transition between the deep and shallow marine environments [Orme et al., 2014; An et al., 2014], which formed part of an early Cenozoic syncollisional basin system developed along the IYSZ [e.g., Ding et al., 2005].

In the study area, the Cretaceous sequence is bounded by the Great Counter Thrust (GCT), which comprises two strands in the study area (i.e., on both the northern and southern basin boundaries, see Figure 2), forming a wide, asymmetric synclinorium striking W-E, with a 6–8 km wide southern flank and a 10–15 km wide northern flank [Wang et al., 2012] (Figure 2). The northern GCT defines the boundary between the preserved Xigaze basin sequences and the Kailas Group, specifically the Qiuwu-Dazhuka Formation [Wang et al., 2013; Li et al., 2017] (Figures 2 and 4), extending to the east (Zedang; Figure 1) active during ~19–15 Ma [Quidelleur et al., 1997; Harrison et al., 2000] and to the west (Kailas; Figure 1) active between ~20 and 13 Ma [Yin et al., 1999]. Furthermore, Carrapa et al. [2014] suggested that the northern strand of the GCT (Figure 2) probably ceased to be active ~17 Ma. The southern GCT preserves an imbricated thrust, comprising from north to south the Xigaze basin sequences, Liuqu Formation, Xigaze ophiolite, and the northern Tethyan Himalaya sequences structurally overlying one another (Figures 2 and 4). Based on strain analysis and restored sections, Einsele et al. [1994] proposed that the preserved basin segment had been shortened 65% of the original width from at least 65 km. Two upper Oligocene-Miocene conglomerates lie on the northern and southern boundaries of the Xigaze basin; the Kailas Group, specifically the Qiuwu-Dazhuka Formation to the north [Wang et al., 2013; Li et al., 2017]; and the coeval Liuqu Formation to the south [Davis et al., 2002; Li et al., 2015a; Leary et al., 2016] (Figures 2 and 4).

4. Sampling and Methods

Nine sandstones and a felsic dyke (T13-20) were sampled along an N-S transect of the Xigaze fore-arc basin (mainly Chongdui and Ngamring Formations) as well as a sandstone sample from the adjacent Qiuwu-Dazhuka Formation (Figure 2; the same transect studied for biostratigraphy by *Wan et al.* [1998] and sedimentation and structure by *Einsele et al.* [1994] and *Wang et al.* [2012]). U-Pb zircon analyses were carried out to determine the maximum depositional age of sediments, as well as the age of felsic dyke emplacement. Furthermore, low-T thermochronology data were used to elucidate both the burial and exhumation history of the basin. Sample T12-66, located near the core of synclinorium, is from the youngest strata in the preserved section of the Xigaze fore-arc basin sequence (Figure 2), while sample T13-22 is from the Qiuwu-Dazhuka Formation.

To constrain the depositional ages of these sequences, we carried out detrital zircon U-Pb analyses, using an Agilent 7700 quadrupole inductively coupled plasma mass spectrometer with a 193 nm ArF Excimer laser at the School of Earth Sciences, The University of Melbourne. Details of the experimental method used are described in the Appendix [*Woodhead et al.*, 2007; *Hellstrom*, 2008; *Paton et al.*, 2010].

Low-T thermochronology methods, e.g., AFT, AHe, and ZHe, have different ranges of temperature sensitivity, termed the partial annealing/retention zone (AHe: ~40–80°C; AFT: ~60–120°C; ZHe: ~130–200°C), and can be applied to determine the rate and timing of cooling of geological units in the upper crustal environment [e.g., *Gleadow et al.*, 2002; *Flowers et al.*, 2009]. Samples in this study were crushed and treated by traditional mineral separation techniques (heavy liquid and magnetic separation) to separate the apatite and zircon grains. AFT, AHe, and ZHe analyses were conducted on samples at the University of Melbourne. Details of these low-T thermochronology analytical procedures are described in the supporting information [*Farley et al.*, 1996; *Flowers et al.*, 2009; *Gleadow et al.*, 2015].

5. Results

5.1. U-Pb Detrital Zircon Chronology

In total, 696 subhedral or rounded zircon grains (80 to 250 μm) from six samples were analyzed for constraining the depositional ages of the Xigaze fore-arc basin sequences, which yielded 645 concordant U-Pb ages (Figure 5 and supporting information). The southernmost sample T12-59 yielded 87 concordant U-Pb ages ranging between 3427 and 105 Ma. The youngest age group (14 grains) falls between ~107 and 105 Ma with a weighted mean age of $\sim 106 \pm 0.8$ Ma (Figure 5), providing a maximum depositional age constraint for the lower part of the Ngamring Formation. Sample T12-60 yielded 101 concordant ages ranging from ~3260 to 101 Ma with a youngest age peak of $\sim 102 \pm 0.9$ Ma (eight grains), from the slightly younger sequence of lower part of the Ngamring Formation. Sample T12-61 yielded 118 concordant ages ranging from 2260 to 97 Ma with a youngest age peak of $\sim 98.8 \pm 1.1$ Ma (five grains), while sample T12-65 yielded 111 concordant ages ranging from 2157 to 90 Ma with a youngest age peak of $\sim 90.5 \pm 1.5$ Ma (four grains). Sample T12-66 from the youngest sequence (synclinorium core) yielded concordant ages of 3281–82 Ma with youngest age peak of $\sim 82.9 \pm 1.0$ Ma (four grains), while sample T13-19-1 from the northern flank yielded 115 concordant ages in range of 2733–93 Ma with a youngest age peak of $\sim 94.2 \pm 0.8$ Ma (seven grains). Worthy of note is that in sample T12-61 the youngest detrital U-Pb age measured is $\sim 98.8 \pm 1.1$ Ma (see supporting information), which is slightly older than the previous biostratigraphic Turonian age for this strata [*Wan et al.*, 1998]. This implies that there may be slightly younger zircons in this unit that have not been recorded in our analyses (Figure 3). Generally, the youngest peaks of detrital U-Pb ages from these samples show a younging trend of the sedimentary sequences from the northern and southern flanks to the synclinorium core (Figure 3), consistent with previous biostratigraphic study [*Wan et al.*, 1998]. Furthermore, the sample (T13-20) from the felsic dyke on the northern flank has a concordant zircon U-Pb age of $\sim 14.84 \pm 0.11$ Ma (Figure 6).

5.2. AFT Data

Eleven samples were analyzed for AFT by using the "RadialPlotter" (Figure 7) [Vermeesch, 2009], and each only displays one single age peak, which is always considerably younger than its age of deposition (Figures 3 and 5). AFT pooled ages of eight sedimentary rocks from the N-S transect (N-S) in the Xigaze fore-arc basin range from $\sim 62.6 \pm 3.2$ to $\sim 16.3 \pm 1.5$ Ma and generally show a pattern of northward

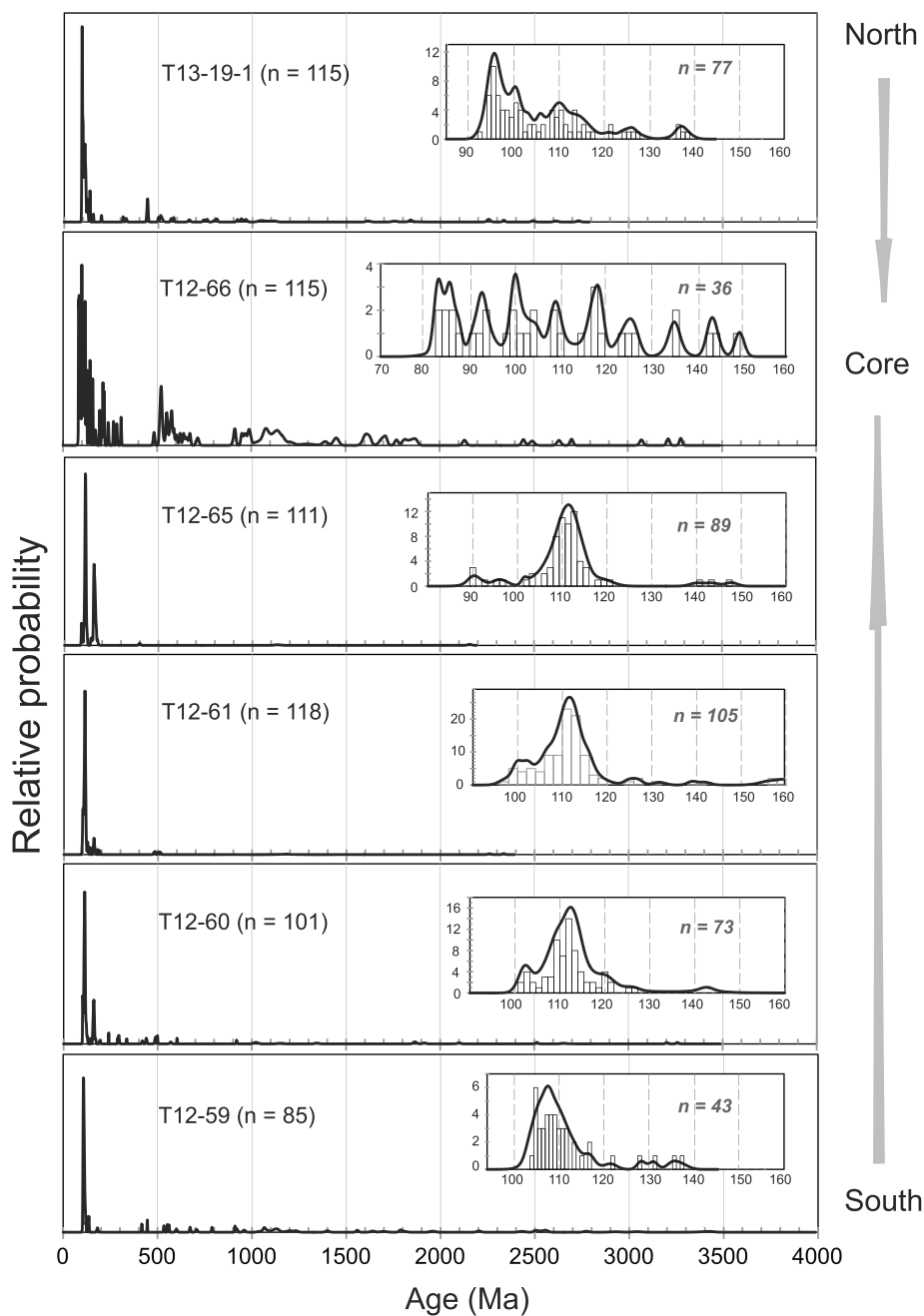


Figure 5. Plots of detrital zircon U-Pb age probability from the Xigaze fore-arc sequence.

younging (Figure 7). Slightly older ages in samples T13-19-1 and T13-19-2 at higher elevation (>4200 m) compared to samples T12-65 and T12-66 located in close proximity but at slightly lower elevations (around 4000 m) are probably a result of earlier cooling of the higher elevation samples (Table 1). The relatively short track lengths range between 10.8 and 11.9 μm for the mean length (Table 1), showing that these samples were buried within the partial annealing zone of AFT or reheated for a long period before exhuming to the near surface environment. The AFT age of $\sim 15.0 \pm 1.0$ Ma from sample T13-22, collected from the late Oligocene-Miocene Qiuwu-Dazhuka Formation, is consistent with data previously published previously from the same unit located near Kailas [Carrapa et al., 2014]. The felsic dyke sample (T12-20) yielded a pooled AFT age at $\sim 15.0 \pm 2.0$ Ma, comparable (within analytical error) with the coexisting zircon U-Pb age of $\sim 14.84 \pm 0.11$ Ma (Figure 6).

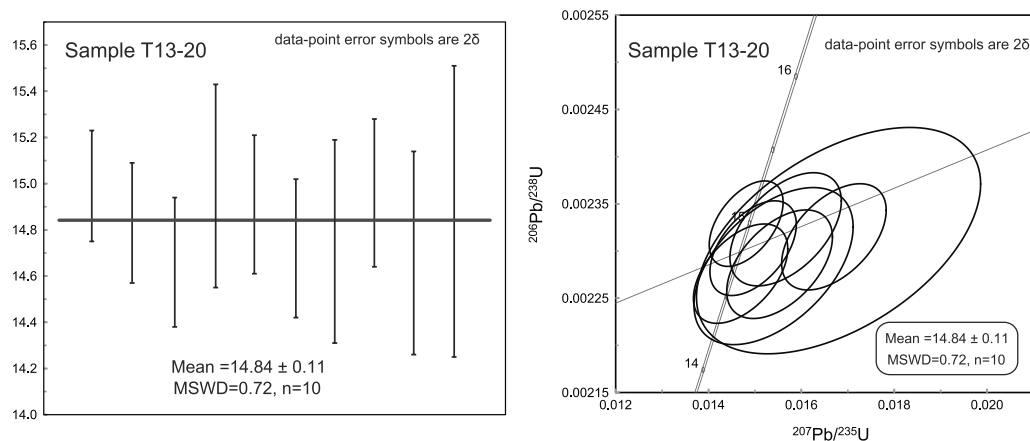


Figure 6. Weighted average of ^{206}Pb -corrected ages and concordia plot from sample T13-20. MSWD = mean square of weighted deviate.

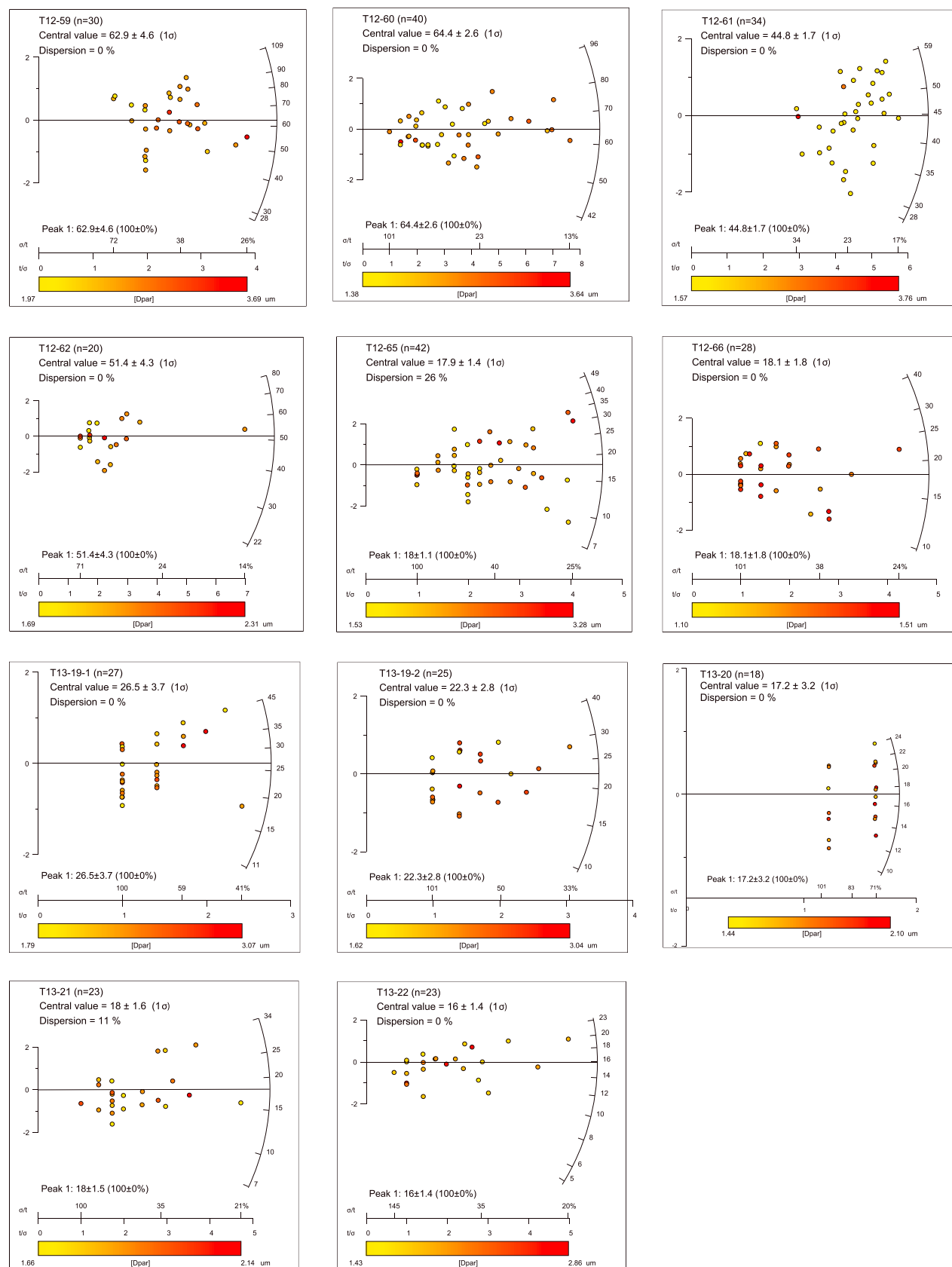
5.3. AHe Data

A total of 21 grains from six samples (two to four grains for each sample) were analyzed for AHe dating, which have [eU] values ranging from 2.3 to 55.1 ppm (Table 2) without clear relationships between their ages and [eU] (see Figure S1 in the supporting information). All grains yielded reproducible Miocene AHe ages, ranging between $\sim 15.0 \pm 1.1$ and 7.7 ± 0.5 Ma (Table 2), considerably younger than their own corresponding AFT and depositional ages. Samples T12-65 and T12-66 at lower elevations, from the youngest strata near the core of the synclinorium at ~ 3900 m, yielded the youngest AHe ages of 7.7 ± 0.5 and 8.2 ± 2.3 Ma, respectively, whereas other samples located on the flanks at slightly higher elevations (~ 4000 – 4700 m) yield slightly older ages (Tables 1 and 2).

5.4. ZHe Data

Six sandstones samples (T12-59, T1260, T12-61, T12-62, T12-65, and T13-19-1) from Xigaze fore-arc basin strata as well as sample T13-22 from the Qiuwu-Dazhuka Formation were selected for ZHe dating. Three to seven grains were analyzed for each sample (28 grains in total), and most grains have relatively low [eU] values, < 700 ppm, except for one grain (1225 ppm) of sample T13-22 (Table 3). However, this high [eU] grain, which might be expected to show the effects of enhanced He diffusion [Guenther *et al.*, 2013], yielded an age of $\sim 17.3 \pm 1.1$ Ma. Considering the analytical error, this is concordant with ages of other grains from sample T13-22 (Table 3). Sample T12-59 yielded seven dispersed ZHe ages in the range of $\sim 89.8 \pm 5.3$ – 57.3 ± 3.6 Ma, while sample T12-60 yielded five dispersed ZHe ages falling between $\sim 92.5 \pm 5.7$ and 53.4 ± 3.3 . The single grain ages of the two samples are all younger than their depositional ages, indicating that they were partially reset. A further four samples from the Xigaze fore-arc basin yielded reproducible ages from Late Cretaceous to early Miocene, with weighted mean ages in the range of $\sim 72.0 \pm 6.7$ – 24.6 ± 1.8 Ma, while a sample (T12-22) from Qiuwu-Dazhuka Formation yielded an age of $\sim 18.0 \pm 1.3$ Ma (weighted mean age; Table 3).

In general, AFT, AHe, and ZHe ages from the sandstones are all significantly younger than their depositional ages and are considered to have been totally reset following deposition, except for the ZHe ages for the two southernmost samples (T12-59 and T12-60), which are considered to have been only partially reset (Figures 3 and 5 and Tables 1–3). These low-T thermochronology age data are consistent with their different expected temperature sensitivities, ZHe > AFT > AHe. The spatial and temporal distributions of the ZHe and AFT ages show a similar northward younging pattern, while AHe results from samples consistently yield Miocene ages (Figure 8). This pattern prevails despite samples having been located at different elevations ranging from 3900 to 4700 m; hence, their ages are considered to have been mainly controlled by their location within the basin. Of note is that the four samples from the narrow southernmost basin area (~ 5 – 6 km wide) yield pre-Oligocene ZHe and AFT ages, while all others to the north all yield Miocene ages.

**Figure 7.** Radial plots of the apatite FT ages using the RadialPlotter [Vermeesch, 2009].

Sample No.	Locality (°E/N)	Elevation (m)	No. of Grains (n)	Age Results					Track Length and DPAR Results				
				Spontaneous Tracks					Projected				
				No. (n)	Density (10 cm ⁻²) ^d	^a Pooled ²³⁸ U (ppm)	^b Pooled Age (Ma ± 1SD)	^c P(χ ²)	^b Dispersion (%)	^d Central Age (Ma ± 1SD)	Mean (μm ± 1SD)	Mean (μm ± 1SD)	No. (n) (Range) (μm)
T12-59	88.619/29.122	4135	30	193	1.006	3.21	60.1 ± 3.9	24	0	62.9 ± 4.6	11.1 ± 2.6	12.7 ± 1.6	149 (15–34)
T12-60	88.627/29.128	4090	40	664	4.203	12.25	63.2 ± 2.2	22	0	64.4 ± 2.6	10.8 ± 2.7	12.7 ± 1.5	173 (13–31)
T12-61	88.630/29.132	4052	34	763	2.203	9.53	43.9 ± 1.5	43	0	44.8 ± 1.7	11.9 ± 1.8	13.2 ± 1.3	174 (14–2.8)
T12-62	88.625/29.137	4042	20	159	2.034	7.94	49.1 ± 3.8	35	0	51.4 ± 4.3	10.3 ± 3.2	12.5 ± 1.8	94 (1.3–4.6)
T12-65	88.592/29.171	4076	42	270	1.238	16.54	16.3 ± 1.5	46	26	17.9 ± 1.4	11.9 ± 2.6	13.4 ± 1.5	143 (2.25–3.6)
T12-66	88.590/29.179	4083	28	112	1.765	19.42	17.1 ± 1.7	50	0	18.1 ± 1.8	11.7 ± 3.0	13.2 ± 2.0	100 (1.2–3.2)
T13-19-1	88.721/29.242	4720	27	53	5.432	4.16	24.3 ± 2.2	52	0	26.5 ± 3.7	11.9 ± 2.9	13.3 ± 1.9	55 (1.5–3.7)
T13-19-2	88.724/29.251	4281	25	68	5.879	5.82	20.9 ± 1.8	42	0	22.3 ± 2.8	0	11.5 ± 2.8	23.2 (1.6–3.0)
T13-20	88.735/29.282	3987	18	29	2.129	2.36	15.0 ± 2.0	34	0	16.2 ± 3.2	11.5 ± 2.8	13.2 ± 1.7	126 (1.7–2.3)
T13-21	88.766/29.307	3912	23	142	0.951	10.8	16.8 ± 1.7	54	11	18.0 ± 1.6	0	1.7 ± 1.7	1.84 (1.7–2.1)
T13-22	88.772/29.319	3891	23	143	2.592	34.79	15.0 ± 1.0	55	0	16.0 ± 1.4	0	1.4–2.7	1.93 (1.4–2.7)

^aPooled uranium content of all grains measured by laser ablation inductively coupled plasma mass spectrometry.
^bPooled AFT ages of all grains.
^cP value of χ² for (n – 1) degrees of freedom [Galbraith, 1981].
^dLengths measured after ²⁵²Cf irradiation.
^eC axis projected mean track length after Ketcham et al. [2007].

6. Thermal History Modeling

6.1. Modeling Strategy for Single Samples

Based on our AFT, ZHe, and AHe data and some regional geological constraints, the thermal histories for eight samples were modeled together, employing the inverse method of the HeFTy software [Ketcham, 2005; Ketcham et al., 2007]. Two initial geological constraints are applied for these thermal history modeling: (1) the temperature of 15 ± 5°C for the mean present surface and (2) our new detrital zircon U-Pb ages (the youngest age peaks) and biostratigraphy study published by Wan et al. [1998] are used to constrain depositional ages of samples from the Xigaze basin sequence, while the crystallization age was used for igneous sample T13-20.

Samples T12-59, T12-61, T12-62, T12-65, and T13-19-1 were modeled by using combined ZHe, AHe, and AFT data; the sample T12-66 was modeled with AHe and AFT data by using constraints from ZHe ages of its nearby sample T12-65. AFT data from sample T12-60 were combined with the AHe age of nearby sample T12-59, while sample T13-20 was modeled by using AFT data with constraints from its zircon U-Pb age (Figure 6). For samples T12-59 and T12-60, for ZHe data, broad constraint boxes were used for because of partial resetting for ZHe system (Figure 9). The further modeling strategy is described in detail in the Appendix [Ketcham et al., 2007].

6.2. Results of Thermal History Modeling

Thermal history models of the low-T thermochronology data show that the timing of onset of cooling propagated from south to north (Figures 9 and 10). In the south, Early Cretaceous sediments underwent pronounced cooling between ~89 ± 2 and 80 ± 3 Ma (samples T12-59 and T12-60, located on the southernmost part of the basin; Figure 2), followed by a lengthy slow cooling period until early Miocene time. Samples T12-61 and T12-62 (Cenomanian), located further north, show rapid cooling over an interval

Table 2. Apatite (U-Th)/He Data for Xigaze Forearc Basin

Sample No.	⁴ He ncc	Mass (mg)	^a Mean FT	U ppm	Th ppm	Sm ppm	Th/U	^b [eU] ppm	Corr. Age (Ma)	Error ±1σ	Grain Width (μm)	Grain Length (μm)	^c Weighted Mean age (Ma)
T12-59	0.038	0.0087	0.74	2.1	10.1	108.9	4.87	2.3	10.6	0.7	61.0	161.0	
T12-59	0.035	0.0040	0.71	2.6	20.0	251.8	7.81	3.0	13.4	0.8	53.4	180.6	
T12-59	0.088	0.0141	0.76	2.5	10.6	86.3	4.29	5.0	13.3	0.8	56.0	224.5	
T12-59	0.084	0.0123	0.76	2.5	15.1	131.1	6.10	6.0	11.9	0.7	58.9	174.8	12.2 ± 2.1
T12-61	0.082	0.0086	0.77	4.7	16.2	128.3	3.44	8.5	11.8	0.7	65.9	239.0	
T12-61	0.071	0.0060	0.75	6.3	30.8	202.6	4.92	13.5	9.4	0.6	60.7	161.5	
T12-61	0.125	0.0072	0.76	5.1	27.5	145.0	5.36	11.6	16.0	1.0	67.8	187.7	12.7 ± 4.4
T12-62	0.021	0.0062	0.76	1.3	4.2	33.8	3.20	2.3	15.8	1.0	62.0	159.5	
T12-62	0.027	0.0064	0.76	1.6	6.4	58.8	3.93	3.1	14.0	0.9	58.8	262.5	15 ± 1.1
T12-65	0.078	0.0056	0.75	3.5	68.7	307.9	19.55	19.6	7.5	0.5	60.1	227.7	
T12-65	0.093	0.0035	0.74	23.6	54.1	130.3	2.29	36.3	8.0	0.5	57.7	166.1	
T12-65	0.094	0.0049	0.77	8.3	78.5	256.7	9.43	26.7	7.5	0.5	72.6	161.1	
T12-65	0.041	0.0030	0.71	5.2	63.0	185.1	12.00	20.0	7.9	0.5	51.6	169.7	7.7 ± 0.5
T12-66	0.021	0.0027	0.66	2.6	25.7	138.8	10.07	8.6	11.0	0.7	47.0	149.8	
T12-66	0.088	0.0024	0.66	35.6	82.9	125.4	2.33	55.1	8.2	0.5	45.1	143.8	
T12-66	0.030	0.0040	0.71	6.3	24.7	105.7	3.90	12.1	7.0	0.4	45.9	189.1	
T12-66	0.033	0.0032	0.68	5.2	39.5	183.1	7.56	14.5	8.5	0.5	43.1	236.3	8.2 ± 2.3
T13-19-1	0.063	0.0148	0.81	1.8	4.5	55.4	2.57	2.9	15.1	0.9	67.2	325.7	
T13-19-1	0.047	0.0099	0.78	2.2	10.3	59.5	4.78	4.6	10.6	0.7	63.2	247.2	
T13-19-1	0.034	0.0086	0.76	1.7	8.2	143.8	4.92	3.6	11.1	0.7	66.1	236.6	11.8 ± 3.5

^aα-ejection correction [Farley et al., 1996].^bEffective uranium content, [eU] = [U] + 0.235 × [Th] [Flowers et al., 2009].^cWeighted means at 95% confidence level calculated by using Isoplot V3.0 [Ludwig, 2003].**Table 3.** Zircon (U-Th)/He Data for Xigaze Area

Sample No.	⁴ He ncc	Mass (mg)	Mean FT	U ppm	Th ppm	Th/U	[eU] ppm	Corr. Age (Ma)	Error ±1σ	Grain Width (μm)	Grain Length (μm)	Weighted Mean Age (Ma)
<i>Zircon</i>												
T12-59	3.643	0.0085	0.80	45.0	27.3	0.61	51.4	68.5	4.2	53.3	237.4	
T12-59	7.097	0.0097	0.81	87.8	57.3	0.65	101.3	58.9	3.7	59.2	235.4	
T12-59	13.996	0.0149	0.83	91.3	40.2	0.44	100.7	76.1	4.7	59.5	313.2	
T12-59	20.360	0.0136	0.83	128.0	58.9	0.46	141.8	85.9	5.3	63.0	276.3	
T12-59	11.100	0.0087	0.80	103.2	54.1	0.52	115.9	89.8	5.6	56.2	230.0	
T12-59	5.894	0.0100	0.82	67.8	32.8	0.48	75.5	63.6	3.9	58.3	243.6	
T12-59	3.652	0.0051	0.77	90.4	49.9	0.55	102.1	57.3	3.6	49.0	185.6	
T12-60	1.969	0.0104	0.81	266.2	109.7	0.65	292.0	53.4	3.3	54.8	266.2	
T12-60	9.867	0.0049	0.74	248.0	73.2	0.48	265.2	80.8	5.0	36.6	248.0	
T12-60	23.322	0.0098	0.78	211.4	168.6	0.80	265.1	77.5	4.8	44.5	331.1	
T12-60	8.312	0.0048	0.77	179.9	91.2	0.51	201.3	68.5	4.3	95.2	192.1	
T12-60	7.784	0.0073	0.80	211.4	108.9	0.49	237.0	92.5	5.7	54.4	211.4	
T12-61	10.038	0.0091	0.80	121.8	44.9	0.37	132.4	68.0	4.2	51.4	260.3	
T12-61	28.744	0.0168	0.82	194.6	129.2	0.66	225.0	62.1	3.8	54.9	380.5	
T12-61	22.073	0.0205	0.84	113.8	50.0	0.44	125.6	70.1	4.3	63.8	363.2	66.4 ± 2.4
T12-62	11.081	0.0079	0.76	87.5	97.4	1.11	110.4	69.2	4.3	80.3	320.9	
T12-62	24.951	0.0069	0.78	344.3	225.0	0.65	397.1	74.4	4.6	57.1	235.7	
T12-62	15.900	0.0027	0.69	571.4	387.0	0.68	662.3	72.7	4.5	31.5	191.8	72.0 ± 6.7
T12-65	7.927	0.0164	0.83	98.8	58.4	0.59	112.6	35.2	2.2	60.9	326.3	
T12-65	5.010	0.0096	0.80	111.2	73.8	0.66	128.5	33.5	2.1	54.5	252.3	34.3 ± 3.0
T13-19-1	1.305	0.0069	0.79	63.6	40.9	0.64	73.2	21.4	1.3	51.5	213.9	
T13-19-1	6.688	0.0089	0.80	178.8	113.8	0.64	205.5	30.1	1.9	50.6	260.1	
T13-19-1	0.921	0.0066	0.78	37.5	31.4	0.84	44.9	25.7	1.6	50.6	211.4	24.6 ± 1.8
T13-22	27.399	0.0105	0.82	1125.8	457.8	0.41	1233.4	17.3	1.1	57.9	253.4	
T13-22	6.114	0.0144	0.83	183.2	126.2	0.69	212.9	16.3	1.0	68.3	266.0	
T13-22	9.065	0.0067	0.78	402.8	396.0	0.98	495.8	22.5	1.4	58.5	222.8	18.0 ± 1.3

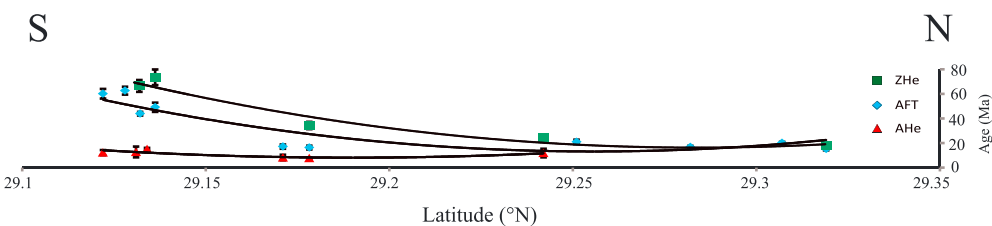


Figure 8. Plot of thermochronology ages ($\pm 1\sigma$) for samples versus latitude along the transect S-N in Figure 2. Dispersed ZHe ages for the two southernmost samples are not shown. GCT = Great Counter Thrust.

from $\sim 65 \pm 3$ to 52 ± 3 Ma, followed by slow cooling through to early Miocene time. By contrast, four samples (T12-65, T12-66, T13-19-1, and T13-19-2, Turonian-Santonian) from the central and northern Xigaze basin experienced a prolonged heating history through to latest Eocene time ($\sim 34 \pm 3$ Ma), followed by rapid Oligocene cooling (Figures 6 and 7). All samples record pronounced cooling commencing in the middle Miocene ($\sim 14 \pm 2$ Ma; Figures 9 and 10). Note that pre-Oligocene cooling episodes are only recorded by samples located on the narrow southern basin flank.

7. Discussion

7.1. Time Span of the Xigaze Basin

Currently, the Xigaze basin sequences expose two types of deposit: the fore-arc and overlying syncollisional basin sequence along the Indian-Asian collisional zone. These sedimentary archives record the processes of pre- and syn-Indian-Asian collision. In the study area, however, only the fore-arc sequences consisting of the Aptian (~113 to 110 Ma) Chongdui Formation without the radiolarian chert unit [An *et al.*, 2014; Huang *et al.*, 2015; Wang *et al.*, 2017] and Albian-Santonian (~110 to 83 Ma) Ngamring Formation (Figure 3) have been preserved. Our new U-Pb zircon data from the Ngamring Formation generally support previous studies on the deposition age of the Xigaze fore-arc sequences near Xigaze (Figures 3 and 5). To the west, the younger deposits, known as the Campanian to Ypresian (~82 to 50 Ma) Tso-jiangding Group, have been preserved in the Zhongba-Saga areas (Figure 1). Based on recent studies, the initial India-Asia collision probably occurred at ~ 60 Ma [e.g., DeCelles *et al.*, 2014; Hu *et al.*, 2015, 2016a]. In this case, the later sequence in Xigaze basin could be defined as a collision-related syncollisional basin [Hu *et al.*, 2016a, 2016b], currently mainly including the youngest unit, the Lower Eocene Jialazi Formation near Zhongba which consists of the limestone interlayered with thin sandstone and conglomerate sequences [e.g., Orme *et al.*, 2014; Hu *et al.*, 2015, 2016a]. The preservation of Eocene strata provides evidence that deposition in the basin continued after initial collision.

Furthermore, recent low-temperature thermochronology studies indicate that a considerable section was removed from the entire India-Asia collisional zone during Miocene [Carrapa *et al.*, 2014; Li *et al.*, 2015a, 2015c]. Hence, Eocene strata were probably deposited over the entire Xigaze basin. Because the basin form is a gentle syncline with no record of significant Eocene structural activity, the heating observed in thermal history models is probably attributed to continued sedimentary accumulation caused by the northward migration of the basin depocenter until latest Eocene time, rather than by folding and/or faulting. The termination of heating is coeval with the last recorded regional marine sedimentation to the south in Yadong [Jiang *et al.*, 2016], as well as in Gyangze [Li *et al.*, 2005] (although the timing of this marine sequence is still under debate; Figure 1), which probably indicates that in southern Tibet the remnant Neo-Tethyan Sea finally terminated at that time. Thus, we propose that deposition in the Xigaze basin continued until latest Eocene or earliest Oligocene time and that the upper sequence was subsequently eroded.

7.2. Cooling and Exhumation History of the Xigaze Basin

As mentioned above, samples with pre-Oligocene apparent ZHe and AFT ages and cooling episodes are only located in a narrow zone along the southern basin margin, while others (located in the central and northern parts) all show Miocene ages and Oligocene-Miocene cooling. This spatial pattern in the cooling/exhumation history is attributed to the early geometrical architecture of the Xigaze basin during its deposition. Recently, Noda [2016] reviewed characteristics of present-day compressional fore-arc basin systems that have an

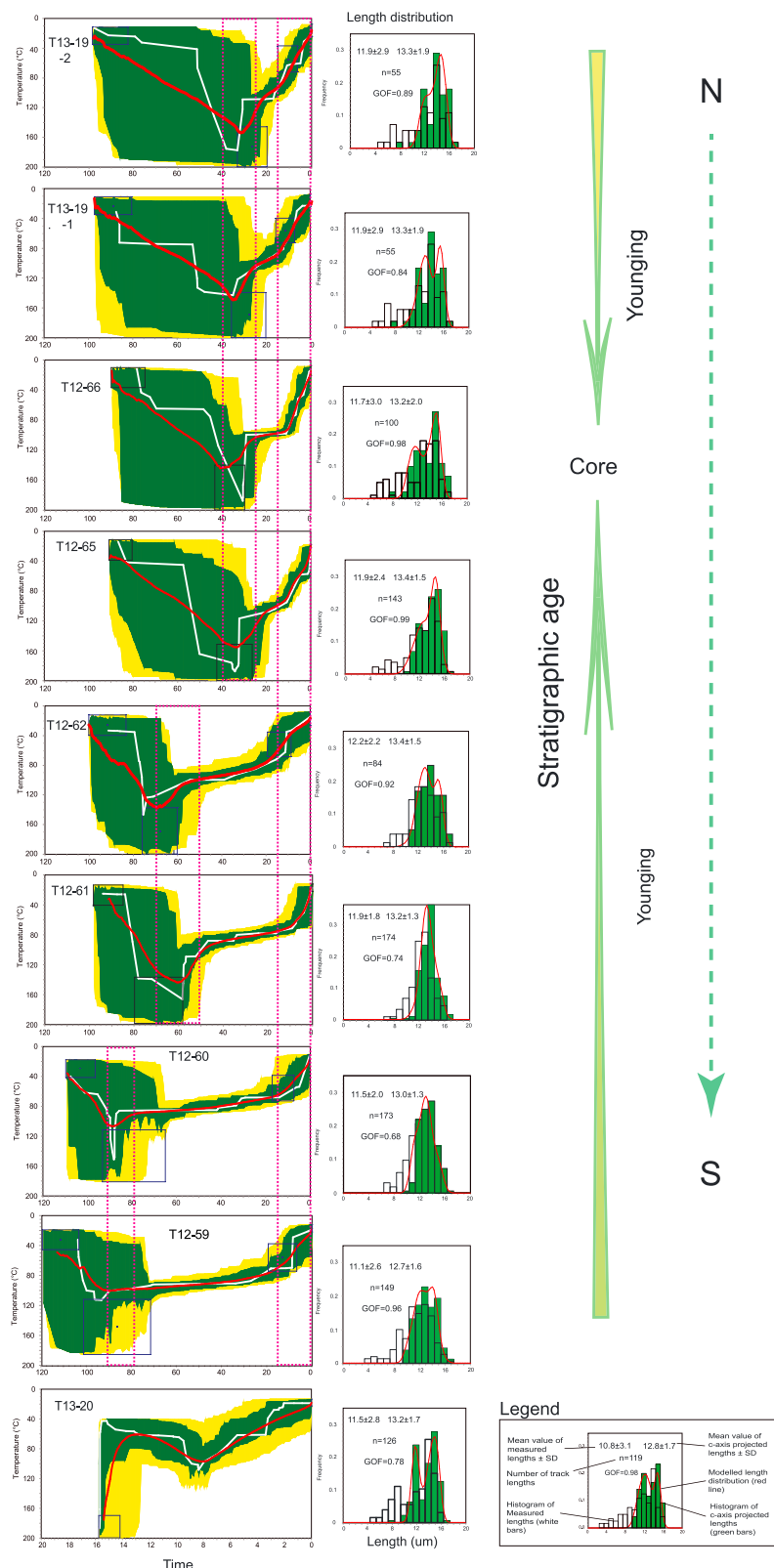


Figure 9. Thermal history modeling results of samples from the study area. Constraints are shown as black boxes. (left) “Good” paths ($GOF > 0.55$) shown as dark green envelopes and “acceptable” paths ($GOF > 0.05$) as yellow envelopes. The red line represents the weighted mean thermal path for all good models, and a white line is the best fit thermal path for each sample. (right) Length distribution histograms (see legend for further details). GOF = goodness of fit.

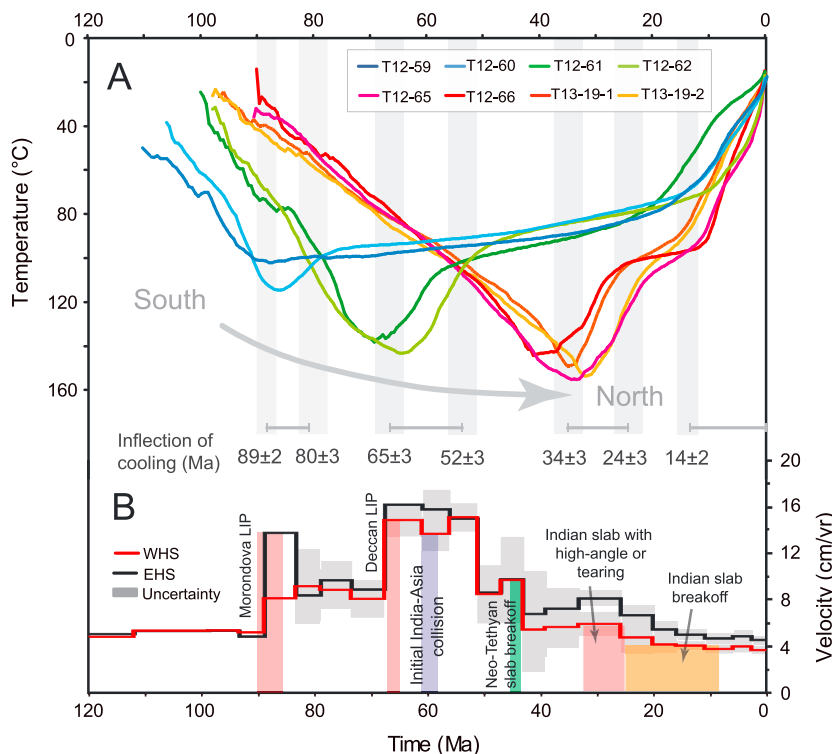


Figure 10. (a) Weighted mean thermal paths for samples from the Xigaze basin (as shown in Figure 9) display a northward younging cooling trend. The grey bars mark the timing of onset of cooling episodes. (b) Relative India-Asia convergent velocities of Eastern/Western Himalayan Syntaxis (E/WHS) from ~120 Ma to present [van Hinsbergen et al., 2011a] showing timing of the Morondova and Deccan LIPs, Initial India-Asia collision [DeCelles et al., 2014; Hu et al., 2015], Neo-Tethys slab breakoff [Ji et al., 2016], Indian slab tearing [Zhang et al., 2014], and Indian slab breakoff reflected by ultrapotassic magmatism of the southern Lhasa terrane [Tian et al., 2017]; LIP = Large Igneous Province.

asymmetric “listric” geometry and developed through landward migration of the basin depocenter. We propose a similar structural model for the Xigaze basin with a “listric” geometry and landward migrating depocenter during Late Cretaceous (Figure 11). This model is also consistent with its present asymmetric synclinorium profile (Figure 2b). Further, the termination of postdepositional heating propagating from south to north is also considered to correlate with northward migration of the Xigaze basin depocenter (Figure 11).

In detail, the temporal record of cooling in the Xigaze basin correlates with significant, independently constrained observations, relevant to the developing collision dynamics. The onset of cooling (at $\sim 89 \pm 2$

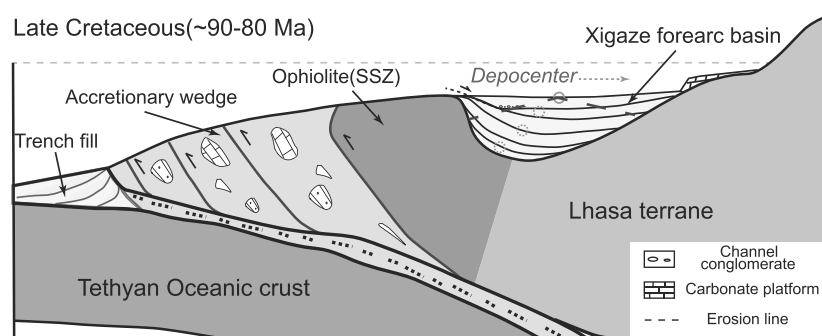


Figure 11. Tectonic model for southern Asian margin in Tibet during ~90–80 Ma. The Xigaze basin had an asymmetric listric geometry with northward migration of the depocenter (dashed circles), resulting in rapid exhumation of the southern basin; SSZ = suprasubduction zone.

and 80 ± 3 Ma) in the southernmost basin was accompanied by thrusting (probably representing early activity of the YZMT [Ding *et al.*, 2005]) or uplift of the accretionary wedge and ophiolites along its southern margin. We relate this uplift/exhumation episode with accelerated northward convergence and anticlockwise rotation of the Indian plate relative to Asia between ~ 90 and 80 Ma, which has been attributed to Morondova Large Igneous Province (LIP) activity and drag of Neo-Tethyan slab subduction [van Hinsbergen *et al.*, 2011a] (Figure 10). Acceleration and rotation of India led to a changing pattern of Neo-Tethyan slab subduction and/or possible regional stress during that time, which triggered thrusting of the accretionary wedge and ophiolitic basement and exhumation of the southernmost Xigaze basin. Further, the occurrence of the unconformable conglomerate layer in the southern basin (Figure 4a4) is a response of this period of exhumation in the southernmost portion, although it was previously interpreted as a deepwater channel [Wang *et al.*, 2012].

Further north, the cooling episode from $\sim 65 \pm 3$ to 52 ± 3 Ma also coincided with a period of the fastest India-Asia convergence possibly linked to the activity of the Deccan LIP and traction of fast Neo-Tethyan subduction [van Hinsbergen *et al.*, 2011a, 2011b] (Figure 10). Similar to the earlier exhumation described above, this second episode is attributed to continued thrusting along the YZMT [Ding *et al.*, 2005], resulting in propagation exhumation further north within the basin. Subsequent slow cooling probably relates to the significant decrease in convergence that accompanied ongoing India-Asia collision. Based on sedimentary provenance analysis, Hu *et al.* [2015, 2016a] and DeCelles *et al.* [2014] argued for initial collision in southern Tibet at $\sim 59 \pm 1$ Ma. However, no significant decrease of the convergence rate is apparent at that time, possibly due to accommodation by subduction of the Indian lithosphere and “softer” upper crustal shortening.

In the central and northern basins, continuous heating revealed by our thermal modeling is attributed to continued sedimentary accumulation in the basin until latest Eocene time. The subsequent pronounced Oligocene cooling, probably linked to the crustal flexure, was related to Indian slab high-angle subduction or tearing [Zhang *et al.*, 2014]. This was also accompanied by a period of slightly accelerated Indian convergence (Figure 10). Later slow to minimal early Miocene cooling was probably associated with the proposed decrease in subduction angle of the Indian slab following its breakoff as recorded by contemporary ultrapotassic magmatism in southern Lhasa [Tian *et al.*, 2017] (Figure 10). This cooling pattern coincides with a slightly decrease in the India-Asia convergence at that time (~ 25 – 15 Ma) [van Hinsbergen *et al.*, 2011a].

In keeping with previous regional findings (Figure 1), for example, Kailas area [Carrapa *et al.*, 2014], the southern Gangdese belt [Copeland *et al.*, 1995; Dai *et al.*, 2013; Tremblay *et al.*, 2015; Li *et al.*, 2016; Ge *et al.*, 2017], Liuqu Formation [Li *et al.*, 2015a], and Zedang area in southeast Tibet [Li *et al.*, 2015c], all apatite samples analyzed here show pronounced cooling since middle Miocene time (Figures 9 and 10). The modern Yarlung River system has also been incising the IYSZ at least since that time [Cina *et al.*, 2009]. Hence, the Miocene cooling phase is here attributed to post-thrust (GCT) erosion and Yarlung River incision.

Recently, low-T thermochronology data (e.g., ZFT, AFT, ZHe, and AHe) were reported by Dai *et al.* [2013] and Ge *et al.* [2017] from the Gangdese batholith near Xigaze located to the north of this study area. They suggested that the northern Gangdese batholith (from $N29.5^\circ$ to the north) experienced late Eocene-early Oligocene exhumation, which might have been triggered by crustal thickening followed by the Neo-Tethyan slab breakoff. By contrast, the southern Gangdese batholith only recorded the late Oligocene-early Miocene fast cooling, which may be a result of denudation related to the late Oligocene Gangdese Thrust or regional extension. By the early Miocene, the rapid exhumation is considered to have associated with localized Yarlung river incision [Li *et al.*, 2016] (Figure 1). Therefore, it appears that the exhumation/cooling history of the Xigaze basin differs from that of the Gangdese arc to the north. We propose that the Xigaze basin is a relatively “soft” unit, located within the collision zone, and was therefore more sensitive to the effects of India-Asia convergence (e.g., thrusting and/or folding), compared to the more distal and relative “rigid” Gangdese batholith further north.

7.3. Implication for Evolution of India-Asia Convergence

In summary, our study shows that the geological evolution of the Xigaze basin between Early Cretaceous (~ 113 Ma) and latest Eocene (~ 34 Ma) time carries a unique record of both fore-arc and syncollisional basin systems in the course of the India-Asia convergence. To the south, the Indian plate initially separated from

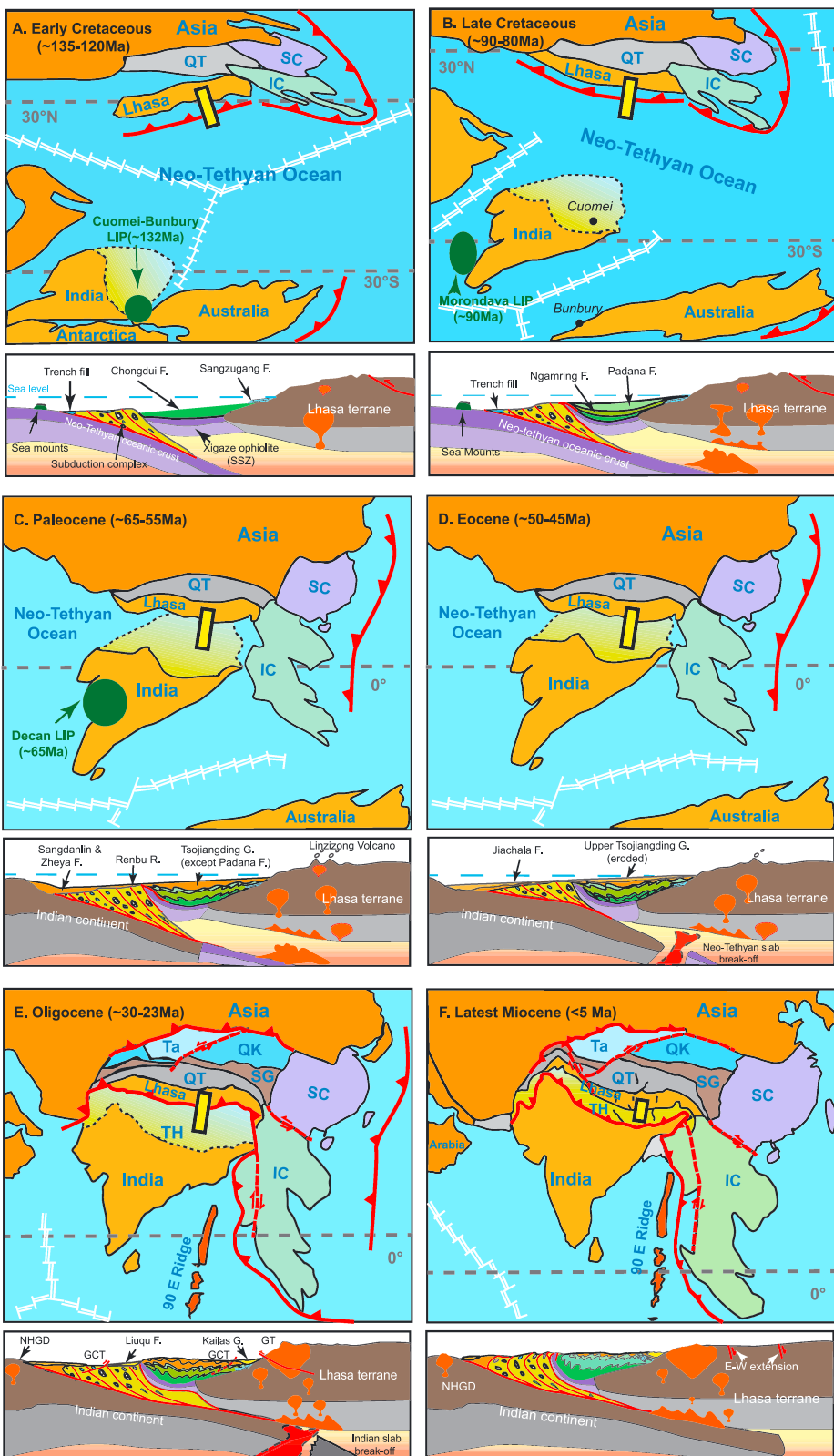


Figure 12. Schematic Early Cretaceous to present paleogeographic evolution of the Tibetan Plateau. The yellow bar in each panel represents the cross-section locations. GCT = Great Counter Thrust, GT = Gangdese Thrust, NHGD = Northern Himalayan gneiss domes, LIP = Large Igneous Province, SSZ = suprasubduction zone, F./G. = formation/group, IC = Indochina, QK = Qaidam-Kunlun, QT = Qiangtang, SC = South China, SG = Songpan-Ganzi, Ta = Tarim.

eastern Gondwana (Australian continent) at ~132 Ma (Early Cretaceous), in response to the activity of the Cuomei-Bunbury LIP [Zhu *et al.*, 2013] and demonstrated by marine magnetic anomalies [Müller *et al.*, 2008]. To the north, the Xigaze fore-arc basin was initially deposited on oceanic crust adjacent to the southern Asian continental margin, fed by increasing volumes of Gangdese arc-derived sediments (Figure 12a). From ~90 Ma, acceleration of the northward movement and rotation of the Indian plate triggered rapid thrusting of the underlying accretionary wedge and ophiolites. This resulted in exhumation/uplift of the southernmost part of the basin at that time and was accompanied by northward movement of its depocenter (Figures 10 and 12b). The Gangdese arc also records a strong magmatism at that time which is related to Neo-Tethyan subduction [Ji *et al.*, 2009].

In the early Paleocene, the high convergence rate between the Indian and Asian plates from ~65 to 50 Ma led to a further episode of uplift of the southern basin and initial collision between India and Asia. This resulted in extensive shortening (by folding) of the sedimentary sequences (Figure 12c), and deceleration of the Indian plate is only recorded after ~50 Ma, following this “soft collision” stage. Since then, dramatically decrease of the convergence rate between India and Asia was accompanied by activity of the Tethyan Himalayan fold-thrust belt [Ratschbacher *et al.*, 1994; Murphy and Yin, 2003; Ding *et al.*, 2005] and high-temperature metamorphism in Tethyan Himalaya commencing at ~50 Ma [Lee *et al.*, 2000; Lee and Whitehouse, 2007], as well as a coeval episode of Gangdese magmatism between ~60 and 45 Ma [e.g., Ji *et al.*, 2009, 2016; Zhu *et al.*, 2009]. Hence, this post ~50 Ma stage can be linked to later “hard collision” related to continental crust collision [Molnar and Tapponnier, 1975; Lee and Lawver, 1995]. During this period, the Xigaze basin transitioned from a fore-arc to collision-related syncollisional basin system in front of the Gangdese arc, and sediment sourced from the Gangdese arc along the south Asian margin was continuously transported into the Xigaze basin (Figures 12c and 12d), as well as to other foreland basins further south (Renbu, Sangdanlin basins [DeCelles *et al.*, 2014; Orme *et al.*, 2014; Li *et al.*, 2015b] Figure 12c).

Following Neo-Tethyan slab breakoff by ~45 Ma [Replumaz *et al.*, 2010; Ji *et al.*, 2016] (Figure 9d), the Indian lithosphere flat subduction caused strong horizontal compression and deceleration of India-Asia convergence and contributed to formation and uplift of the central Tibetan Plateau (Qiangtang and Lhasa terranes in Figure 1) [Rohrmann *et al.*, 2012; Li *et al.*, 2016]. This led to further development of crustal thickening of the Tethyan Himalaya [Zeng *et al.*, 2011], as well as southward migration of the foreland basin system. Sedimentation of the Xigaze syncollisional basin finally terminated by $\sim 34 \pm 4$ Ma, and the remnant Neo-Tethyan Sea in south Tibet finally closed.

After latest Eocene time, with continued India-Asia convergence and increasing high-angle subduction and breakoff of the India slab, the Xigaze basin experienced rapid uplift and erosion, leading to removal of the uppermost syncollisional basin sequence. During the latest Oligocene-early Miocene, two fluvial basins (Kailas and Liuqu) were formed in local structural depressions along the north and south boundaries of the Xigaze basin (Figure 12e) [Li *et al.*, 2015b; Leary *et al.*, 2016]. At that time, the Xigaze ophiolite was exposed and, together with Xigaze basin strata, provided the source for the Liuqu Formation (to the south) and Kailas Group (to the north). In the early Miocene, following Indian slab breakoff, enhanced crustal uplift and shortening activated extrusion of the Himalaya (MCT and STD activities) and movement of the GCT [Yin, 2006], resulting in ophiolite thrusting over the Xigaze and fluvial basins. This led to cessation of sedimentation in fluvial basins and also localized the modern Yarlung drainage system with accompanying widespread denudation [Carrapa *et al.*, 2014; Li *et al.*, 2015c]. Furthermore, the Tibetan Plateau has been undergoing the E-W extension since the Miocene [e.g., Yin, 2006] and been being shaped by both tectonic and climatic forces (Figure 12f).

8. Conclusions

In the study area, the Xigaze fore-arc/syncollisional basin preserves a unique record of Cretaceous and Cenozoic India-Asia convergence. Combining the results of new U-Pb zircon data with previous studies confirms that sedimentary units preserved in the Xigaze basin and studied here range in age from ~113 to 80 Ma and represent a fore-arc sequence.

New low-T thermochronology data from an N-S section across the Xigaze fore-arc basin near Xigaze generally show a northward younging age-trend, consistent with a northward propagating heating and cooling thermal history pattern. An early episode of cooling occurred in the southern basin from ~90 to 80 Ma and

was followed by a later fast cooling episode between ~65 and 50 Ma, whereas the central and northern Xigaze basin experienced a longer burial history until the latest Eocene (~35 Ma). This burial represents a substantial collision-related sedimentary sequence deposited until ~35 Ma, which has since been removed but is partially preserved in the basin at >300 km to the west.

Late Cretaceous-Oligocene cooling/exhumation episodes recorded in the Xigaze basin relate to thrusting and folding associated with changes in India-Asia convergence rates. The later pronounced rapid Miocene cooling episode, which is widespread across the region, is related to post-thrust (GCT) erosion and incision by the Yarlung River. These temporal and spatial relationships indicate that surface processes within the orogenic belt are strongly coupled with dynamic activity of the deep crust.

Acknowledgments

This study was financially supported by grants from the China National Nature Science Foundation (41430212) and the ARC Discovery Early Career Research Award (DE120102245), as well as the AuScope Program of NCRIS. Abaz Alimanovic is acknowledged for his assistance with AHe and ZHe analyses. The authors thank Devon A. Orme and Editors Douwe van Hinsbergen and Uri ten Brink for their constructive reviews and helpful suggestions. Further data for this paper are available by contacting the corresponding author at guangwei.li@unimelb.edu.au.

References

- Aitchison, J. C., A. M. Davis, Badengzhu, and H. Luo (2003), The Gangdese Thrust: A phantom structure that did not raise Tibet, *Terra Nova*, 15(3), 155–162.
- An, W., X. Hu, E. Garzanti, M. K. Boudagher-Fadel, J. Wang, and G. Sun (2014), Xigaze forearc basin revisited (south Tibet): Provenance changes and origin of the Xigaze ophiolite, *Geol. Soc. Am. Bull.*, 126(11–12), 1595–1613.
- An, W., X. Hu, and E. Garzanti (2017), Sandstone provenance and tectonic evolution of the Xiukang Mélange from Neotethyan subduction to India-Asia collision (Yarlung-Zangbo suture, south Tibet), *Gondwana Res.*, 41, 222–234, doi:10.1016/j.gr.2015.08.010.
- Armstrong, P. A. (2005), Thermochronometers in sedimentary basins, in *Low-Temperature Thermochronology: Techniques, Interpretations, and Applications*, Rev. Mineral. Geochem., vol. 58, edited by P. W. Reiners and T. A. Ehlers, pp. 499–520, Mineral. Soc. of Am., Washington, D. C.
- Cao, R. (1991), Sedimentology of trench-arc sediments and its relation to ophiolite obduction, *Phys. Chem. Earth*, 18, 237–268, doi:10.1016/0079-1946(91)90003-X.
- Carrapa, B., D. Orme, P. DeCelles, P. Kapp, M. Cosca, and R. Waldrip (2014), Miocene burial and exhumation of the India-Asia collision zone in southern Tibet: Response to slab dynamics and erosion, *Geology*, 42(5), 443–446.
- Cina, S. E., A. Yin, M. Grove, C. S. Dubey, D. P. Shukla, O. M. Lovera, T. K. Kelty, G. E. Gehrels, and D. A. Foster (2009), Gangdese arc detritus within the eastern Himalayan Neogene foreland basin: Implications for the Neogene evolution of the Yalu-Brahmaputra River system, *Earth Planet. Sci. Lett.*, 285, 150–162.
- Copeland, P., T. M. Harrison, Y. Pan, W. S. F. Kidd, M. Roden, and Y. Q. Zhang (1995), Thermal evolution of the Gangdese batholith, southern Tibet: A history of episodic unroofing, *Tectonics*, 14, 223–236, doi:10.1029/94TC01676.
- Dai, J., C. Wang, J. Hourigan, Z. Li, and G. Zhuang (2013), Exhumation history of the Gangdese batholith, southern Tibetan plateau: Evidence from apatite and zircon (U-Th)/He thermochronology, *J. Geol.*, 121(2), 155–172.
- Davis, A. M., J. C. Aithison, D. Z. Bai, H. Luo, and S. Zyabrev (2002), Paleogene island arc collision-related conglomerates, Yarlung-Tsangpo suture zone, Tibet, *Sediment. Geol.*, 150(3–4), 247–273.
- DeCelles, P., P. Kapp, J. Quade, and G. E. Gehrels (2011), Oligocene-Miocene Kailas basin, southwestern Tibet: Record of postcollisional upper plate extension in the Indus-Yarlung Suture Zone, *Geol. Soc. Am. Bull.*, 123, 1337–1362, doi:10.1130/B30258.1.
- DeCelles, P., P. Kapp, G. Gehrels, and L. Ding (2014), Paleocene-Eocene foreland basin evolution in the Himalaya of southern Tibet and Nepal: Implications for the age of initial India-Asia collision, *Tectonics*, 33, 824–849, doi:10.1002/2014TC003522.
- Ding, L., P. Kapp, and X. Wan (2005), Paleocene-Eocene record of ophiolite obduction and initial India-Asia collision, south central Tibet, *Tectonics*, 24, TC3001, doi:10.1029/2004TC001729.
- Dürer, S. B. (1996), Provenance of Xigaze fore-arc basin clastic rocks (Cretaceous, south Tibet), *Geol. Soc. Am. Bull.*, 108(6), 669–684.
- Einsele, G., B. Liu, S. Dürer, W. Frisch, G. Liu, H. Luterbacher, L. Ratschbacher, W. Ricken, J. Wendt, and A. Wetzel (1994), The Xigaze forearc basin: Evolution and facies architecture (Cretaceous, Tibet), *Sediment. Geol.*, 90(1), 1–32.
- Farley, K. A., R. A. Wolf, and L. T. Silver (1996), The effects of long alpha-stopping distances on (U-Th)/He ages, *Geochim. Cosmochim. Acta*, 60(21), 4223–4229.
- Flowers, R. M., R. A. Ketcham, D. L. Shuster, and K. A. Farley (2009), Apatite (U-Th)/He thermochronometry using a radiation damage accumulation and annealing model, *Geochim. Cosmochim. Acta*, 73, 2347–2365.
- Galbraith, R. F. (1981), On statistical models for fission track counts, *Math. Geol.*, 13, 471–488.
- Garver, J. I., M. T. Brandon, M. Roden-Tice, and P. J. J. Kamp (1999), Erosional denudation determined by fission-track ages of detrital apatite and zircon, in *Exhumation Processes: Normal Faulting, Ductile Flow, and Erosion*, edited by U. Ring et al., *Geol. Soc. London, Spec. Publ.*, 154, 283–304.
- Garzanti, E. (1999), Stratigraphy and sedimentary history of the Nepal Tethys Himalaya passive margin, *J. Asian Earth Sci.*, 17, 805–827.
- Garzanti, E., and T. van Haver (1988), The Indus clastics: Forearc basin sedimentation in the Ladakh Himalaya (India), *Sediment. Geol.*, 59(3), 237–249.
- Ge, Y. K., J. G. Dai, C. S. Wang, Y. L. Li, G. Q. Xu, and M. Danisik (2017), Cenozoic thermo-tectonic evolution of the Gangdese batholith constrained by low-temperature thermochronology, *Gondwana Res.*, 41, 451–462, doi:10.1016/j.gr.2016.05.006.
- Gleadow, A., D. X. Belton, B. P. Kohn, and R. W. Brown (2002), Fission track dating of phosphate minerals and the thermochronology of apatite, *Rev. Mineral. Geochem.*, 48(1), 579–630.
- Gleadow, A., M. Harrison, B. Kohn, R. Lugo-Zazueta, and D. Phillips (2015), The Fish Canyon Tuff: A new look at an old low-temperature thermochronology standard, *Earth Planet. Sci. Lett.*, 424, 95–108.
- Guenther, W. R., P. W. Reiners, R. A. Ketcham, L. Nasdala, and G. Giester (2013), Helium diffusion in natural zircon: Radiation damage, anisotropy, and the interpretation of zircon (U-Th)/He thermochronology, *Am. J. Sci.*, 313(3), 145–198.
- Harrison, T. M., A. Yin, M. Grove, O. M. Lovera, F. J. Ryerson, and X. Zhou (2000), The Zedong Window: A record of superposed Tertiary convergence in southeastern Tibet, *J. Geophys. Res.*, 105, 19,211–19,230, doi:10.1029/2000JB900078.
- Hébert, H., R. Bezard, C. Guillette, J. Dostal, C. S. Wang, and Z. F. Liu (2012), The Indus-Yarlung Zangbo ophiolites from Nanga Parbat to Namche Barwa syntaxes, southern Tibet: First synthesis of petrology, geochemistry, and geochronology with incidences on geodynamic reconstructions of Neo-Tethys, *Gondwana Res.*, 22(2), 3777–3397.
- Hellstrom, J. (2008), Iolite: Software for spatially resolved LA-(quad and MC) ICPMS analysis, in *Laser Ablation ICP-MS in the Earth Sciences: Current Practices and Outstanding Issues*, edited by P. Sylvester, pp. 343–348, Mineralogical Association of Canada, Québec Quebec Canada.

- Hu, X., E. Garzanti, T. Moore, and I. Raffi (2015), Direct stratigraphic dating of India-Asia collision onset at the Selandian (middle Paleocene, 59 ± 1 Ma), *Geology*, 43(10), 859–862.
- Hu, X., E. Garzanti, J. Wang, W. Huang, W. An, and A. Webb (2016a), The timing of India-Asia collision onset—Facts, theories, controversies, *Earth Sci. Rev.*, 160, 264–299.
- Hu, X., J. Wang, M. BouDagher-Fadel, E. Garzanti, and W. An (2016b), New insights into the timing of the India-Asia collision from the Paleogene Quxia and Jialazi formations of the Xigaze forearc basin, south Tibet, *Gondwana Res.*, 32, 76–92, doi:10.1016/j.gr.2015.02.007.
- Huang, W., D. J. J. van Hinsbergen, M. Maffione, D. A. Orme, G. Dupont-Nivet, C. Guilmotte, and P. Kapp (2015), Lower Cretaceous Xigaze ophiolites formed in the Gangdese forearc: Evidence from paleomagnetism, sediment provenance, and stratigraphy, *Earth Planet. Sci. Lett.*, 415, 142–153, doi:10.1016/j.epsl.2015.01.032.
- Jadoul, F., F. Berra, and E. Garzanti (1998), The Tethys Himalayan passive margin from Late Triassic to Early Cretaceous (south Tibet), *J. Asian Earth Sci.*, 16(2), 173–194.
- Ji, W. Q., F. Y. Wu, S. L. Chung, J. X. Li, and C. Z. Liu (2009), Zircon U-Pb geochronology and Hf isotopic constraints on petrogenesis of the Gangdese batholith, southern Tibet, *Chem. Geol.*, 262(3–4), 229–245.
- Ji, W. Q., F. Y. Wu, S. L. Chung, X. C. Wang, C. Z. Liu, Q. L. Li, and J. G. Wang (2016), Eocene Neo-Tethyan slab breakoff constrained by 45 Ma oceanic island basalt-type magmatism in southern Tibet, *Geology*, G37612, 37,611.
- Jiang, T., J. C. Aitchison, and X. Wan (2016), The youngest marine deposits preserved in southern Tibet and disappearance of the Tethyan Ocean, *Gondwana Res.*, 32, 64–75, doi:10.1016/j.gr.2015.01.015.
- Ketcham, R. A. (2005), Forward and inverse modeling of low-temperature thermochronometry data, *Rev. Mineral. Geochem.*, 58, 275–314.
- Ketcham, R. A., A. Carter, R. A. Donelick, J. Barberand, and A. J. Hurford (2007), Improved measurement of fission-track annealing in apatite using c-axis projection, *Am. Mineral.*, 92, 789–798.
- Leary, R., D. A. DeCelles, P. J. Quade, G. E. Gehrels, and G. Waanders (2016), The Liuqu Conglomerate, southern Tibet: Early Miocene basin development related to deformation within the Great Counter Thrust system, *Lithosphere*, doi:10.1130/L542.1.
- Lee, T., and L. A. Lawver (1995), Cenozoic plate reconstruction of Southeast Asia, *Tectonophysics*, 251, 85–183.
- Lee, J., and M. J. Whitehouse (2007), Onset of mid-crustal extensional flow in southern Tibet: Evidence from U/Pb zircon ages, *Geology*, 35, 45–48.
- Lee, J., W. S. Dinklage, B. R. Hacker, Y. Wang, P. B. Gans, A. Calvert, J. Wan, W. Chen, A. Blythe, and W. McClelland (2000), Evolution of the Kangmar Dome, southern Tibet: Structural, petrologic, and thermochronologic constraints, *Tectonics*, 19, 872–896, doi:10.1029/1999TC001147.
- Lee, J., B. Hacker, and Y. Wang (2004), Evolution of North Himalayan gneiss domes: Structural and metamorphic studies in Mabja Dome, southern Tibet, *J. Struct. Geol.*, 204, 2297–2316.
- Li, G. B., X. Q. Wan, W. Liu, D. Liang, and Y. Hyesu (2005), Discovery of Paleogene marine stratum along the southern side of Yarlung-Zangbo suture zone and its implications in tectonics, *Sci. China Ser. D Earth Sci.*, 48(5), 647–661.
- Li, J. G., Z. Y. Guo, D. J. Batten, H. W. Cai, and Y. Y. Zhang (2010), Palynological stratigraphy of the Late Cretaceous and Cenozoic collision-related conglomerates at Qiabulin, Xigaze, Xizang (Tibet) and its bearing on palaeoenvironmental development, *J. Asian Earth Sci.*, 38, 86–95.
- Li, G., B. Kohn, M. Sandiford, Z. Xu, and L. Wei (2015a), Constraining the age of Liuqu Conglomerate, southern Tibet: Implications for evolution of the India-Asia collision zone, *Earth Planet. Sci. Lett.*, 426, 259–266.
- Li, G., M., Sandiford, S., Boger, X., Liu, and L., Wei (2015b), Provenance of the Upper Cretaceous to lower Tertiary sedimentary relicts in the Renbu Melange Zone, within the Indus-Yarlung Suture Zone, *J. Geol.*, 123(1), 39–54. doi:10.1086/680207
- Li, G., Y. Tian, B. P. Kohn, M. Sandiford, Z. Xu, and Z. Cai (2015c), Cenozoic low temperature cooling history of the northern Tethyan Himalaya in Zedang, SE Tibet and its implications, *Tectonophysics*, 643, 80–93.
- Li, G., B. Kohn, M. Sandiford, Z. Xu, Y. Tian, and C. Seiler (2016), Synorogenic morphotectonic evolution of the Gangdese batholith, south Tibet: Insights from low-temperature thermochronology, *Geochem. Geophys. Geosyst.*, 17, 101–112, doi:10.1002/2015GC006047.
- Li, S., L. Ding, Q. Xu, H. Wang, Y. Yue, and U. Baral (2017), The evolution of Yarlung Tsangpo River: Constraints from the age and provenance of the Gangdese Conglomerates, southern Tibet, *Gondwana Res.*, doi:10.1016/j.gr.2015.05.010.
- Liu, C. J., J. X. Yin, X. X. Sun, and Y. Y. Sun (1988), Marine Late Cretaceous-early Tertiary sequences: The nonflysch deposits of the Xigaze forearc basin in south Xizang [in Chinese], *Mém. Inst. Geol. Acad. Sin.*, 3, 130–157.
- Liu, G., and G. Einsele (1994), Sedimentary history of the Tethyan basin in the Tibetan Himalayas, *Geol. Rundsch.*, 83, 32–61.
- Ludwig, K. R. (2003), *User's Manual for Isoplot 3.0: A Geochronological Toolkit for Microsoft Excel*, Spec. Publ., vol. 4, Berkeley Geochronology Center, Berkeley.
- Maffione, M., D. J. J. van Hinsbergen, L. M. T. Koornneef, C. Guilmotte, K. Hodges, N. Borneman, W. Huang, L. Ding, and P. Kapp (2015), Forearc hyperextension dismembered the south Tibetan ophiolites, *Geology*, 43(6), 475–478.
- Malpas, J., M. F. Zhou, P. T. Robinson, and P. H. Reynolds (2003), Geochemical and geochronological constraints on the origin and emplacement of the Yarlung Zangbo ophiolites, southern Tibet, *Geol. Soc. London, Spec. Publ.*, 218, 191–206.
- McQuarrie, N., S. P. Long, T. Tobgay, J. N. Nesbit, G. Gehrels, and M. N. Ducea (2013), Documenting basin scale, geometry and provenance through detrital geochemical data: Lessons from the Neoproterozoic to Ordovician Lesser, Greater, and Tethyan Himalayan strata of Bhutan, *Gondwana Res.*, 23, 1491–1510, doi:10.1016/j.gr.2012.09.002.
- Molnar, P., and P. Tapponnier (1975), Cenozoic tectonics of Asia: Effects of a continental collision, *Science*, 189, 419–426.
- Müller, R. D., M. Sdrolias, C. Gaina, and W. R. Roest (2008), Age, spreading rates and spreading symmetry of the world's ocean crust, *Geochem. Geophys. Geosyst.*, 9, Q04006, doi:10.1029/2007GC001743.
- Murphy, M. A., and A. Yin (2003), Structural evolution and sequence of thrusting in the Tethyan fold-thrust belt and Indus-Yalu suture zone, southwest Tibet, *Geol. Soc. Am. Bull.*, 115, 21–34.
- Noda, A. (2016), Forearc basins: Types, geometries, and relationships to subduction zone dynamics, *Geol. Soc. Am. Bull.*, 128, 879–895.
- Orme, D. A., B. Carrapa, and P. Kapp (2014), Sedimentology, provenance and geochronology of the Upper Cretaceous-lower Eocene western Xigaze forearc basin, southern Tibet, *Basin Res.*, 27(4), 387–411.
- Orme, D. A., and A. K. Laskowski (2016), Basin analysis of the Albian-Santonian Xigaze Forearc, Lazi region, south-central Tibet, *J. Sediment. Res.*, 86(8), 894–913.
- Parrish, R., and K. V. Hodges (1996), Isotopic constraints on the age and provenance of the Lesser and Greater Himalayan sequences, Nepalese Himalaya, *Geol. Soc. Am. Bull.*, 108, 904–911.
- Paton, C., J. D. Woodhead, J. C. Hellstrom, J. M. Hergt, A. Greig, and R. Maas (2010), Improved laser ablation U-Pb zircon geochronology through robust downhole fractionation correction, *Geostand. Geoanal. Res.*, 31(4), 331–343.
- Pullen, A., P. Kapp, P. G. DeCelles, G. E. Gehrels, and L. Ding (2011), Cenozoic anatexis and exhumation of Tethyan sequence rocks in the Xiao Gurla Range, Southwest Tibet, *Tectonophysics*, 501, 28–40.

- Quidelleur, X., M. Grove, O. M. Lovera, T. M. Harrison, A. Yin, and F. J. Ryerson (1997), Thermal evolution and slip history of the Renbu Zedong Thrust, southeastern Tibet, *J. Geophys. Res.*, 102, 2659–2679, doi:10.1029/96JB02483.
- Ratschbacher, L., W. Frisch, G. Liu, and C. Chen (1994), Distributed deformation in southern and western Tibet during and after the India-Asia collision, *J. Geophys. Res.*, 99, 19,817–19,945, doi:10.1029/94JB00932.
- Replumaz, A., A. M. Negredo, A. Villasenor, and S. Guillot (2010), Indian continental subduction and slab break-off during Tertiary collision, *Terra Nova*, doi:10.1111/j.1365-3121.2010.00945.x.
- Rohrmann, A., P. Kapp, B. Carrapa, P. W. Reiners, J. Guynn, L. Ding, and M. Heizler (2012), Thermochronologic evidence for plateau formation in central Tibet by 45 Ma, *Geology*, 40(2), 187–190.
- Schärer, U., R. H. Xu, and C. J. Allegre (1984), U-Pb geochronology of Gangdese (Transhimalaya) plutonism in the Lhasa-Xigaze region, Tibet, *Earth Planet. Sci. Lett.*, 69, 311–320.
- Tian, S., Z. S. Yang, Z. Q. Hou, X. X. Mo, W. J. Hu, Y. Zhao, and X. Y. Zhao (2017), Subduction of the Indian lower crust beneath southern Tibet revealed by the post-collisional potassic and ultrapotassic rocks in SW Tibet, *Gondwana Res.*, 41, 29–50, doi:10.1016/j.gr.2015.09.005.
- Tremblay, M. M., M. Fox, J. L. Schmidt, A. Tripathy-Lang, M. M. Wielicki, T. M. Harrison, and D. L. Shuster (2015), Erosion in southern Tibet shut down at ~10 Ma due to enhanced rock uplift within the Himalaya, *Proc. Natl. Acad. Sci.*, doi:10.1073/pnas.1515652112.
- van Hinsbergen, D. J., B. Steinberger, P. V. Doubrovine, and R. Gassmöller (2011a), Acceleration and deceleration of India-Asia convergence since the Cretaceous: Roles of mantle plumes and continental collision, *J. Geophys. Res.*, 116, B06101, doi:10.1029/2010JB008051.
- van Hinsbergen, D. J., P. Kapp, G. Dupont-Nivet, P. C. Lippert, P. G. DeCelles, and T. H. Torsvik (2011b), Restoration of Cenozoic deformation in Asia and the size of Greater India, *Tectonics*, 30, TC5003, doi:10.1029/2011TC002908.
- Vermeesch, P. (2009), RadialPlotter: A Java application for fission track, luminescence and other radial plots, *Radiat. Meas.*, 44(4), 409–410.
- Wan, X. Q., L. Wang, C. S. Wang, and L. Jansa (1998), Discovery and significance of Cretaceous fossils from the Xigaze forearc basin, Tibet, *J. Asian Earth Sci.*, 16(2), 217–224.
- Wang, C., X. Li, Z. Liu, Y. Li, L. Jansa, J. Dai, and Y. Wei (2012), Revision of the Cretaceous-Paleogene stratigraphic framework, facies architecture and provenance of the Xigaze forearc basin along the Yarlung Zangbo suture zone, *Gondwana Res.*, 22(2), 415–433.
- Wang, J., X. M. Hu, E. Garzanti, and F. Y. Wu (2013), Upper Oligocene-lower Miocene Gangrinboche Conglomerate in the Xigaze area, southern Tibet: Implications for Himalayan Uplift and Paleo-Yarlung-Zangbo Initiation, *J. Geol.*, 121(4), 425–444.
- Wang, J., X. M. Hu, E. Garzanti, W. An, and X. C. Liu (2017), The birth of the Xigaze forearc basin in southern Tibet, *Earth Planet. Sci. Lett.*, 465, 38–47.
- Woodhead, J. D., J. Hellstrom, J. M. Hergt, A. Greig, and R. Maas (2007), Isotopic and elemental imaging of geological materials by laser ablation inductively coupled plasma-mass spectrometry, *Geostand. Geoanal. Res.*, 31(4), 331–343.
- Wu, F. Y., W. Q. Ji, C. Z. Liu, and S. L. Chung (2010), Detrital zircon U-Pb and Hf isotopic data from the Xigaze fore-arc basin: Constraints on Transhimalayan magmatic evolution in southern Tibet, *Chem. Geol.*, 271(1–2), 13–25.
- Wu, F. Y., W. Q. Ji, J. G. Wang, C. Z. Liu, S. L. Chung, and P. D. Clift (2014), Zircon U-Pb and Hf isotopic constraints on the onset time of India-Asia collision, *Am. J. Sci.*, 314(2), 548–579.
- Yin, A., and T. M. Harrison (2000), Geologic evolution of the Himalayan-Tibetan orogeny, *Annu. Rev. Earth Planet. Sci.*, 28, 211–280.
- Yin, A. (2006), Cenozoic tectonic evolution of the Himalayan orogen as constrained by along strike variation of structural geometry, exhumation history, and foreland sedimentation, *Earth Sci. Rev.*, 76, 1–131.
- Yin, A., T. M. Harrison, M. Murphy, M. Grove, S. Nie, F. Ryerson, and C. Le (1999), Tertiary deformation history of southeastern and southwestern Tibet during the Indo-Asian collision, *Geol. Soc. Am. Bull.*, 111(11), 1644–1664.
- Zeng, L., L. E. Gao, K. Xie, and J. Liu-Zeng (2011), Mid-Eocene high Sr/Y granites in the Northern Himalayan gneiss domes: Melting thickened lower continental crust, *Earth Planet. Sci. Lett.*, 303 (3), 251–266.
- Zhang, L. Y., M. N. Ducea, L. Ding, A. Pullen, P. Kapp, and D. Hoffman (2014), Southern Tibetan Oligocene-Miocene adakites: A record of Indian slab tearing, *Lithos*, 210–211, 209–223.
- Zhu, D. C., S. L. Chung, X. X. Mo, Z. D. Zhao, Y. Niu, B. Song, and Y. H. Yang (2009), The 132 Ma Comei-Bunbury large igneous province: Remnants identified in present-day southeastern Tibet and southwestern Australia, *Geology*, 37(7), 583–586.
- Zhu, D. C., Z. D. Zhao, Y. Niu, Y. Dilek, Z. Q. Hou, and X. X. Mo (2013), The origin and pre-Cenozoic evolution of the Tibetan Plateau, *Gondwana Res.*, 23(4), 1429–1454, doi:10.1016/j.gr.2012.02.002.
- Ziabrev, S., J. Aitchison, A. Abrajevitch, A. Davis, and H. Luo (2003), Precise radiolarian age constraints on the timing of ophiolite generation and sedimentation in the Dazhuqu terrane, Yarlung-Tsangpo suture zone, Tibet, *J. Geol. Soc. Lond.*, 160(4), 591–599, doi:10.1144/0016-764902-107.